Inorganic Chemistry
Article

Inorg. Chem. **2009**, *48*, 5829–5847 **5829**
DOI: 10.1021/ic900154v

Electronic Structure of the [Tris(dithiolene)chromium]^z ($z = 0, 1-, 2-, 3-$) Electron Transfer Series and Their Manganese(IV) Analogues. An X-ray Absorption Spectroscopic and Density Functional Theoretical Study

Priyabrata Banerjee,[†] Stephen Sproules,*[,†] Thomas Weyhermüller,[†] Serena DeBeer George,*[,‡] and Karl Wieghardt*[,†]

[†] *Max-Planck-Institut für Bioanorganische Chemie, Stiftstrasse 34-36, D-45470 Mülheim an der Ruhr, Germany, and*
[‡] *Stanford Synchroton Radiation Lightsource, SLAC, Stanford University, Stanford, California 94309*

Received January 23, 2009

From the reaction mixture of 3,6-dichlorobenzene-1,2-dithiol, $H_2(Cl_2\text{-bdt})$, $[CrCl_3(thf)_3]$, and NEt_3 in tetrahydrofuran (thf) in the presence of air, dark green crystals of $[N(n\text{-}Bu)_4]_2[Cr(Cl_2\text{-bdt})_3]$ (S = 1) (**1**) were isolated upon addition of $[N(n\text{-}Bu)_4]Br$. Oxidation of the $AsPh_4^+$ salt of **1** with $[Fc]PF_6$ yielded microcrystals of $[AsPh_4][Cr(Cl_2\text{-bdt})_3]$ ($S = {}^1/_2$) (**2**) whereas the reduction of **1** with sodium amalgam produced light green crystals of $[N(n\text{-}Bu)_4]_3[Cr(Cl_2\text{-bdt})_3]\cdot thf$ ($S = {}^3/_2$) (**3**). The corresponding maleonitriledithiolato complexes $[PPh_4]_2[Cr(mnt)_3]$ (S = 1) (**4**) and $[PPh_4]_3[Cr(mnt)_3]$ ($S = {}^3/_2$) (**5**) have been synthesized. Isoelectronic manganese complexes of **3** and **5**, namely, $[NEt_4]_2[Mn(Cl_2\text{-bdt})_3]$ ($S = {}^3/_2$) (**6**) and $[PPh_4]_2[Mn(mnt)_3]$ ($S = {}^3/_2$) (**7**), have also been prepared. Complexes **1**, **6**, and **7** have been characterized by single crystal X-ray crystallography. Complexes **1**−**7** have been electrochemically studied and their UV−vis and electron paramagnetic resonance spectra (EPR) have been recorded; magnetic properties have been elucidated by temperature-dependent susceptibility measurements. It is shown by chromium K-edge and sulfur K-edge X-ray absorption spectroscopy (XAS) that the oxidation state of the central Cr ion in each compound is the same (+III, d^3) and that all one-electron redox processes are ligand-based, involving one, two, or three ligand π radical monoanions. Complexes **6** and **7** possess a Mn^{IV} ion with three dianionic ligands. The results have been corroborated by broken symmetry (BS) density functional theoretical (DFT) calculations by using the B3LYP functional. Time-dependent DFT calculations have been performed to calculate the metal and sulfur K-pre-edges. It is suggested that the neutral complexes $[Cr(dithiolene)_3]^0$ $S = 0$ possess octahedral rather than trigonal prismatic CrS_6 polyhedra. Three ligand π radicals ($S_{rad} = {}^1/_2$) couple antiferromagnetically to the central Cr(III) ion (d^3) yielding the observed diamagnetic ground state. It is established that the four members of the $[Cr(dithiolene)_3]^z$ (z = 0, 1−, 2−, 3−) electron transfer series are related by ligand-based one-electron transfer processes; for each of the four members it is shown that they contain a central Cr(III) (d^3) ion, and the CrS_6 polyhedron is a (distorted) octahedron.

Introduction

Since the early work of Holm, McCleverty, Gray, and Schrauzer, it has been firmly established that six-coordinate tris(dithiolene)chromium complexes can exist as neutral species, as well as mono-, di-, and trianions.[1−7] They form an electron transfer series where these four species are electrochemically related by reversible one-electron transfer waves in solution; eq 1.

$$\underset{S=0}{[Cr(L)_3]^0} \underset{-e}{\overset{+e}{\rightleftharpoons}} \underset{S={}^1/_2}{[Cr(L)_3]^{1-}} \underset{-e}{\overset{+e}{\rightleftharpoons}} \underset{S=1}{[Cr(L)_3]^{2-}} \underset{-e}{\overset{+e}{\rightleftharpoons}} \underset{S={}^3/_2}{[Cr(L)_3]^{3-}} \quad (1)$$

The term "dithiolene" (L) will be used for two classes of ligands A and B (shown in Scheme 1) irrespective of their "true" oxidation level as monoanionic radical $(L^{\bullet})^{1-}$, or as dianionic, closed-shell $(L^{Red})^{2-}$ ligand or as neutral 1,2-dithioketone $(L^{Ox})^0$.[8] The ligands and their abbreviations

*To whom correspondence should be addressed. E-mail: sproules@mpi-muelheim.mpg.de (S.S.), debeer@stanford.edu (S.D.G.), wieghardt@mpi-muelheim.mpg.de (K.W.).

(1) Davison, A.; Edelstein, N.; Holm, R. H.; Maki, A. H. *J. Am. Chem. Soc.* **1964**, *86*, 2799.
(2) Schrauzer, G. N.; Mayweg, V. P. *J. Am. Chem. Soc.* **1966**, *88*, 3235.
(3) Wharton, E. J.; McCleverty, J. A. *J. Chem. Soc., A* **1969**, 2258.
(4) Kapre, R. R.; Bothe, E.; Weyhermüller, T.; DeBeer George, S.; Muresan, N.; Wieghardt, K. *Inorg. Chem.* **2007**, *46*, 7827.
(5) Stiefel, E. I.; Bennett, L. E.; Dori, Z.; Crawford, T. H.; Simo, C.; Gray, H. B. *Inorg. Chem.* **1970**, *9*, 281.
(6) McCleverty, J. A.; Locke, J.; Wharton, E. J.; Gerloch, M. *J. Chem. Soc., A* **1968**, 816.
(7) Lewis, G. R.; Dance, I. *J. Chem. Soc., Dalton Trans.* **2000**, 3176.
(8) McCleverty, J. A. *Prog. Inorg. Chem.* **1968**, *10*, 49.

Published on Web 05/26/2009

Scheme 1. Dithiolene Ligands

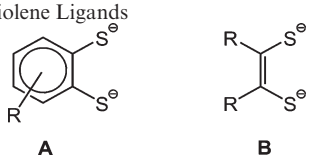

A B

Scheme 2. Ligands and Complexes

Ligands

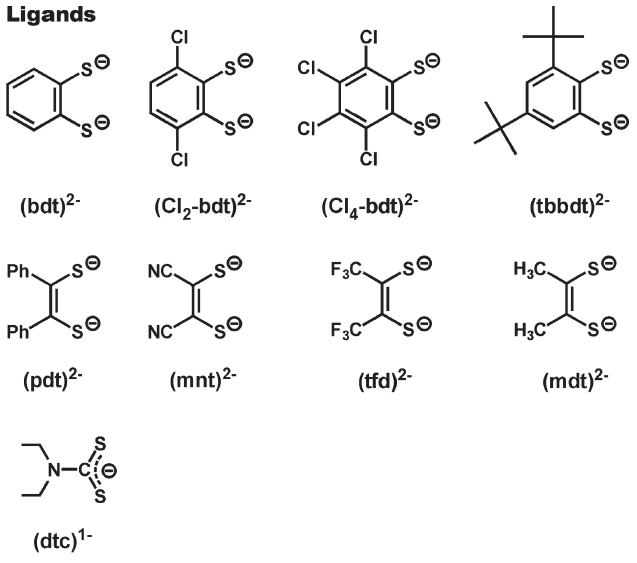

$(bdt)^{2-}$ $(Cl_2\text{-}bdt)^{2-}$ $(Cl_4\text{-}bdt)^{2-}$ $(tbbdt)^{2-}$

$(pdt)^{2-}$ $(mnt)^{2-}$ $(tfd)^{2-}$ $(mdt)^{2-}$

$(dtc)^{1-}$

Complexes

$[Cr^{III}(Cl_2\text{-}bdt)_3][N(n\text{-}Bu)_4]_2 \cdot 2\,CH_2Cl_2 \cdot 2\,CH_3CN$	S = 1	1
$[Cr^{III}(Cl_2\text{-}bdt)_3][AsPh_4]$	S = 1/2	2
$[Cr^{III}(Cl_2\text{-}bdt)_3][N(n\text{-}Bu)_4]_3 \cdot thf$	S = 3/2	3
$[Cr^{III}(mnt)_3][PPh_4]_2$	S = 1	4
$[Cr^{III}(mnt)_3][PPh_4]_3$	S = 3/2	5
$[Mn^{IV}(Cl_2\text{-}bdt)_3][NEt_4]_2 \cdot CH_2Cl_2$	S = 3/2	6
$[Mn^{IV}(mnt)_3][PPh_4]_2$	S = 3/2	7
$[Mn^{III}(dtc)_3]$	S = 2	8
$[Mn^{IV}(dtc)_3][BF_4]$	S = 3/2	9

used in this work are shown in Scheme 2. It is noted that of any given dithiolene ligand no complete [tris(dithiolene) chromium]^z (z = 0, 1−, 2−, 3−) series of complexes has been isolated in the solid state to date.

The following *neutral* species have been isolated and described as diamagnetic, solid materials (S = 0): $[Cr(tfd)_3]^0$ and $[Cr(pdt)_3]^0$.[1,2] There is no crystal structure of such a neutral species. Octahedral[4] and trigonal prismatic[9,10] CrS_6 geometries have been proposed for these neutral complexes. On the other hand, recent density functional theoretical (DFT) calculations on $[Cr^{III}(tbbdt)_3]^0$ (S = 0) point to a distorted octahedral CrS_6 polyhedron with a central Cr(III) ion (S_{Cr} = $^3/_2$) coupled antiferromagnetically to three ligand radicals $(tbbdt^{\bullet})^{1-}$ (S_{rad} = $^1/_2$).[4] Three salts containing a *monoanion* $[Cr(dithiolene)_3]^{1-}$ with an S = $^1/_2$ ground state have been isolated: $[AsPh_4][Cr(tfd)_3]$,[1] and $[NEt_4][Cr(Cl_4\text{-}bdt)_3]$,[3] and $[N(n\text{-}Bu)_4][Cr(tbbdt)_3]$.[4] Only the latter has been structurally characterized by X-ray crystallography. Salts containing a six-coordinate *dianion* $[Cr(dithiolene)_3]^{2-}$ with an S = 1 ground state have also been reported: $[AsPh_4]_2[Cr(tfd)_3]$,[1] and $[AsPh_4]_2[Cr(mnt)_3]$,[1,5,6] which has been structurally characterized.[7] No dianion containing a type A ligand has been isolated previously. The most reduced, *trianionic* $[Cr(dithiolene)_3]^{3-}$ form with an S = $^3/_2$ ground state has been isolated only as $[PPh_4]_3[Cr(mnt)_3]$ salt.[1,6] Its structure has been determined[7] and is the only trianionic tris(mnt) salt to be crystallographically characterized, despite the existence of Fe and Co analogues.[5,6] Again, no complex with a type A dithiolene has been reported. Interestingly, the following dianionic manganese(IV) complexes have also been isolated: $[PPh_4]_2[Mn(mnt)_3]$ and $[N(n\text{-}Bu)_4]_2[Mn(Cl_4\text{-}bdt)_3]$ both of which possess an S = $^3/_2$ ground state,[3,5,6] and only very recently $(PNP)_2[Mn(bdt)_3]$ (PNP^+ = bis(triphenylphosphine)iminium) became the first structurally characterized tris(dithiolene)manganese compound.[11] They are isoelectronic with the corresponding trianions $[Cr(dithiolene)_3]^{3-}$.

The electronic structures of all four members of such a complete $[Cr(dithiolene)_3]^z$ (z = 0, 1−, 2−, 3−) series have not been established. It has recently been spectroscopically shown by electron paramagnetic resonance (EPR) and X-ray absorption near-edge spectroscopy (XANES), in conjunction with density functional theoretical calculations (DFT), that throughout the series $[Cr(tbbdt)_3]^z$ (z = 0, 1−, 2−, 3−) the central metal ion is probably a Cr(III) ion (d^3) and that the redox processes are therefore most likely ligand-centered.[4] Thus, the monoanion $[Cr(tbbdt)_3]^{1-}$ (S = $^1/_2$) contains two ligand π radicals $(tbbdt^{\bullet})^{1-}$ (delocalized), one closed-shell dianion $(tbbdt)^{2-}$, and a central Cr(III) ion confirmed by an XANES study (Cr and S K-edges).[4]

Here, we report a complete investigation of the series $[Cr(Cl_2\text{-}bdt)_3]^{3-,2-,1-}$ (complexes **3**, **1**, **2** shown in Scheme 2) which contain benzene-1,2-dithiolene ligands of type A. We have also investigated two complexes containing type B ligands, namely $[Cr(mnt)_3]^{3-,2-}$ (**5**, **4**).

To study charge and covalency differences we have also prepared and fully characterized two Mn(IV) (d^3) species, namely, $[NEt_4]_2[Mn(Cl_2\text{-}bdt)_3]$ (**6**) and $[PPh_4]_2[Mn(mnt)_3]$ (**7**) which are isoelectronic with the trianions $[Cr(Cl_2\text{-}bdt)_3]^{3-}$ (**3**) and $[Cr(mnt)_3]^{3-}$ (**5**), respectively. Furthermore, we have studied the effect of substituting redox noninnocent ligands of type A and B with relatively redox inert *N*,*N*-diethyldithiocarbamate(1−) ligands in $[Mn^{III}(dtc)_3]^0$ (**8**) and $[Mn^{IV}(dtc)_3]^+$ (**9**).[12,13] Complexes **1**−**9** (Scheme 2) have been investigated by cyclic voltammetry, magnetic susceptibility measurements, EPR and electronic absorption spectroscopies, and by S, Cr, Mn K-edge X-ray absorption spectroscopy (XAS). In addition, we have calculated their structures (geometrical and electronic) by broken symmetry DFT methods. For the first time we show experimentally that

(9) Eisenberg, R.; Stiefel, E. I.; Rosenberg, R. C.; Gray, H. B. *J. Am. Chem. Soc.* **1966**, *88*, 2874.
(10) Schrauzer, G. N.; Finck, H. W.; Mayweg, V. P. *Angew. Chem.* **1964**, *76*, 715.
(11) Lin, C.-H.; Chen, C.-G.; Tsai, M.-L.; Lee, G.-H.; Liaw, W.-F. *Inorg. Chem.* **2008**, *47*, 11435.
(12) (a) Elliot, R. L.; West, B. O.; Snow, M. R.; Tiekink, E. R. T. *Acta Crystallogr.* **1986**, *C42*, 763. (b) Golding, R. M.; Healy, P. C.; Newman, P.; Sinn, E.; Tennant, W. C.; White, A. H. *J. Chem. Phys.* **1970**, *52*, 3105. (c) Saleh, R. Y.; Straub, D. *Inorg. Chem.* **1974**, *13*, 3017. (d) Brown, K. L.; Golding, R. M.; Healy, P. C.; Jessop, K. J.; Tennant, W. C. *Aust. J. Chem.* **1974**, *27*, 2075. (e) Hendrickson, A. R.; Martin, R. L.; Rohde, N. M. *Inorg. Chem.* **1974**, *13*, 1933. (f) Brown, K. L. *Cryst. Struct. Commun.* **1974**, *52*, 3105.
(13) Healy, P. C.; White, A. H. *J. Chem. Soc., Dalton Trans.* **1972**, 1883.

the $[Cr(dithiolene)_3]^{0,1-,2-,3-}$ electron transfer series involves predominantly ligand-based redox chemistry; the central chromium ion retains its +III oxidation state with $(t_{2g})^3$ electron configuration throughout.

Experimental Section

All following syntheses were carried out using standard Schlenk line procedures or a glovebox in the absence of water and dioxygen unless stated otherwise. $Cr^{III}Cl_3(thf)_3$, the ligand $H_2(Cl_2\text{-bdt})$, and $MnCl_2 \cdot 4H_2O$ were purchased from Aldrich and used without further purification. Sodium amalgam (5%) was purchased from Aldrich and washed with *n*-hexane prior to use. Complexes **4** and **5** have been prepared as described in refs 6 and 1, respectively, by using equimolar amounts of $[PPh_4]Br$ instead of $[AsPh_4]Cl$. Similarly, complex **7** was synthesized as described in ref 5. Complexes **8** and **9** were prepared according to ref 12e.

$[N(n\text{-}Bu)_4]_2[Cr^{III}(Cl_2\text{-}bdt^{\bullet})(Cl_2\text{-}bdt)_2] \cdot 2CH_2Cl_2 \cdot 2CH_3CN$ (1). To a solution of the ligand $H_2(Cl_2\text{-bdt})$ (105 mg; 0.50 mmol) in thf (20 mL) under a nitrogen blanketing atmosphere was added triethylamine (140 μL; 1.00 mmol) with stirring. After 10 min $Cr^{III}Cl_3(thf)_3$ (62 mg; 0.17 mmol) was added to the solution at 20 °C. The yellow color of the solution turned dark green. This solution was treated with 2 equiv of tetra-*N*-butylammonium bromide $[N(n\text{-}Bu)_4]Br$ (110 mg; 0.34 mmol) and stirred for 4 h in the presence of air. A green precipitate of **1** formed which was isolated by filtration and washed with diethylether. The compound was recrystallized from a 1:1 dichloromethane/hexane solvent mixture. X-ray quality, dark green single crystals of **1** were obtained from a 1:1 dichloromethane/acetonitrile mixture at −20 °C. Yield: 190 mg (79%). Anal. Calcd for $C_{56}H_{88}N_4S_6Cl_{10}Cr$: C, 47.49; H, 6.21; N, 3.95; S, 13.57; Cr, 3.67. Found: C, 47.45; H, 6.19; N, 3.90; S, 13.54; Cr, 3.62.

$[AsPh_4][Cr^{III}(Cl_2\text{-}bdt^{\bullet})_2(Cl_2\text{-}bdt)]$ (2). To a solution of $[AsPh_4]_2[Cr^{III}(Cl_2\text{-bdt})_3]$ (the $AsPh_4^+$ salt of compound **1**) (0.72 g; 0.50 mmol) in dichloromethane (20 mL) under a nitrogen blanketing atmosphere was added ferrocenium hexafluorophosphate (0.17 g; 0.51 mmol) with stirring at −20 °C. The original dark green color of the solution changed to purple-violet after 1 h. The solvent was removed by evaporation under reduced pressure. The residue was washed 3−4 times with *n*-hexane. The crude compound was extracted with thf and filtered through Celite. Dark violet microcrystals of complex **2** were obtained from a concentrated thf solution at −20 °C. Yield: 0.37 g (70%). Anal. Calcd for $C_{42}H_{26}S_6Cl_6AsCr$: C, 47.46; H, 2.44; S, 18.08; Cr, 4.89. Found: C, 47.48; H, 2.46; S, 18.10; Cr, 4.85.

$[N(n\text{-}Bu_4)]_3[Cr^{III}(Cl_2\text{-}bdt)_3] \cdot C_4H_8O$ (3). To a solution of $[N(n\text{-}Bu_4)]_2[Cr^{III}(Cl_2\text{-bdt})_3]$ (116 mg; 0.10 mmol) in thf (20 mL) under a nitrogen blanketing atmosphere was added Na-amalgam (5%) (46 mg; 0.10 mmol) and 1 equiv of tetrabutylammonium bromide $[N(n\text{-}Bu)_4]Br$ (33 mg; 0.10 mmol) with stirring. The original dark green color of the solution changed to light-green over 3 d. A green precipitate of **3** formed which was collected by filtration and washed with diethylether repeatedly. The product was recrystallized from a 1:1 thf/acetonitrile mixture. Yield: 114 mg (77%). Anal. Calcd for $C_{70}H_{122}N_3S_6Cl_6OCr$: C, 56.87; H, 8.25; N, 2.84; S, 12.99; Cr, 3.52. Found: C, 56.85; H, 8.20; N, 2.81; S, 12.92; Cr, 3.49.

$[NEt_4]_2[Mn^{IV}(Cl_2\text{-}bdt)_3] \cdot CH_2Cl_2$ (6). To a stirring solution of the ligand $H_2(Cl_2\text{-bdt})$ (105 mg; 0.50 mmol) and potassium (39 mg, 1.00 mmol) dissolved in degassed ethanol (4 mL) was added $MnCl_2 \cdot 4H_2O$ (34 mg; 0.17 mmol). The color of the reaction mixture became magenta, and after 30 min in the presence of air, it was filtered into an ethanol solution (20 mL) containing tetraethylammonium bromide (72 mg; 0.34 mmol). Partial evaporation of the solvent under reduced pressure produced a magenta precipitate which was recrystallized from a 1:1 dichloromethane/ethanol mixture to afford dark brown crystals that were washed with diethylether and dried. Yield: 120 mg (69%). Anal. Calcd for $C_{35}H_{48}N_2S_6Cl_8Mn$: C, 40.89; H, 4.67; N, 2.72; S, 18.69; Mn, 5.35. Found: C, 40.81; H, 4.62; N, 2.69; S, 18.62; Mn, 5.29.

X-ray Crystallographic Data Collection and Refinement of the Structures. Single crystals of compounds **1**·CH_3CN, **6**, and **7** were coated with perfloropolyether, picked up with nylon loops, and were immediately mounted in the nitrogen cold stream of a Bruker-Nonius KappaCCD diffractometer equipped with a Mo-target rotating-anode X-ray source. Graphite monochromated Mo Kα radiation (λ = 0.71073 Å) was used throughout. Final cell constants were obtained from least-squares fit of all measured reflections. Intensity data were corrected for absorption using intensities of redundant reflections with the program SADABS.[14] The structures were readily solved by Patterson methods and subsequent difference Fourier techniques. The Siemens ShelXTL[15] software package was used for solution and artwork of the structures; ShelXL97[16] was used for the refinement. All non-hydrogen atoms were anisotropically refined, and hydrogen atoms were placed at calculated positions and refined as riding atoms with isotropic displacement parameters. Crystallographic data of the compounds are listed in Table 1. An *n*-butyl group (C51−C54) of a $[NBu_4]^+$ cation in **1** was found to be disordered and C54 and C53 were split on two positions using equal atomic displacement parameters for corresponding split atoms. C−C bond distances were restrained to be equal within errors.

One of the Cl_2-bdt ligands and an adjacent $[NEt_4]^+$ cation in complex **6** were split on two positions because of disorder. Equal anisotropic displacement parameters were assigned to disordered split atoms S1, S2, and N40 to C48. SIMU and ISOR restraints were necessary to obtain reasonable thermal displacement parameters in the disordered Cl_2-bdt ligand. The geometries of the split fragments were restrained to be equal within errors using the SAME instruction of ShelXL97. The occupation ratio refined to about 0.5:0.5 and was therefore fixed to 0.5 for each part. A total of 427 restraints were used.

Physical Measurements. Electronic spectra of complexes were recorded with a Perkin-Elmer Lambda 19 double-beam spectrophotometer (300−2200 nm). Cyclic voltammograms were recorded with an EG&G potentiostat/galvanostat. Variable temperature (4−300 K) magnetization data were recorded in a 1 T magnetic field on a SQUID magnetometer (MPMS Quantum Design). The experimental magnetic susceptibility data were corrected for underlying diamagnetism using tabulated Pascal's constants. X-band EPR spectra were recorded on a Bruker ESP 300 spectrometer and simulated with ESIM developed by Dr. Eckhard Bill, or with XSophe[17] distributed by Bruker Biospin GmbH. Sulfur and metal K-edge X-ray absorption spectroscopy experiments were conducted at the Stanford Synchrotron Radiation Lightsource under ring conditions of 3.0 GeV and 60−100 mA. The details of experimental data collection and analysis are described in refs 4 and 35, and also given in the Supporting Information. Elemental analyses were performed by H. Kolbe at the Mikroanalytischen Labor in Mülheim an der Ruhr, Germany.

Calculations. All DFT calculations were performed with the ORCA program.[18] The complexes were geometry optimized

(14) *SADABS*, Bruker-Siemens Area Detector Absorption and Other Corrections, Version 2006/1, Sheldrick, G. M., Universität Göttingen: Göttingen, Germany, 2006.
(15) *ShelXTL 6.14*, Bruker AXS Inc., Madison, WI, 2003.
(16) *ShelXL97*, Sheldrick, G. M., Universität Göttingen: Göttingen, Germany, 1997.
(17) Hanson, G. R.; Gates, K. E.; Noble, C. J.; Griffin, M.; Mitchell, A.; Benson, S. *J. Inorg. Biochem.* **2004**, *98*, 903.
(18) Neese, F. *Orca, an Ab Initio, Density Functional and Semiempirical Electronic Structure Program Package*, version 2.6, revision 35; Universität Bonn: Bonn, Germany, 2008.

Table 1. Crystallographic Data for $1 \cdot CH_3CN$, **6**, and **7**

	$1 \cdot CH_3CN$	**6**	**7**
chem. formula	$C_{52}H_{81}Cl_6CrN_3S_6$	$C_{34}H_{46}Cl_6MnN_2S_6$	$C_{60}H_{40}MnN_6P_2S_6$
Fw	1205.26	942.73	1154.22
space group	$P2_1/c$, No. 14	*P-1*, No. 2	*C*2/c, No. 15
a, Å	11.0410(3)	10.9062(8)	28.057(3)
b, Å	21.7366(6)	12.2670(9)	13.4050(12)
c, Å	26.2475(8)	16.8812(8)	19.675(2)
α, deg	90	106.063(6)	90
β, deg	96.716(4)	92.213(6)	129.923(3)
γ, deg	90	107.845(4)	90
V, Å	6256.0(3)	2047.0(2)	5675.0(10)
Z	4	2	4
T, K	100(2)	100(2)	100(2)
ρ calcd, g cm^{-3}	1.280	1.529	1.351
refl. collected/$2\Theta_{max}$	72230/50.00	22237/50.00	77606/66.22
unique refl./$I > 2\sigma(I)$	10975/7900	7176/5184	10774/8256
No. of params/restr.	633/15	551/427	339/0
λ, Å /*μ*(Kα), cm^{-1}	0.71073/6.96	0.71073/10.49	0.71073/5.54
R1 [a]/goodness of fit [b]	0.0779/1.081	0.0628/1.039	0.0401/1.037
wR2 [c] ($I > 2\sigma(I)$)	0.1588	0.1450	0.0976
residual density, e Å^{-3}	+1.00/−0.66	+0.83/−0.82	+0.54/−0.86

[a] Observation criterion: $I > 2\sigma(I)$. $R1 = \sum||F_o| - |F_c||/\sum|F_o|$. [b] $GoF = [\sum[w(F_o^2 - F_c^2)^2]/(n-p)]^{1/2}$. [c] $wR2 = [\sum w(F_o^2 - F_c^2)^2/\sum w(F_o^2)^2]^{1/2}$ where $w = 1/\sigma^2(F_o^2) + (aP)^2 + bP$, $P = (F_o^2 + 2F_c^2)/3$.

using the BP86 functional.[19,20] The all-electron basis sets were those reported by the Ahlrichs group.[21,22] Triple-ζ-quality basis sets with one set of polarization functions (TZVP) were used for metals (Cr and Mn) and sulfur atoms. The remaining atoms were described by slightly smaller polarized split-valence SV(P) basis sets that are double-ζ-quality in the valence region and contain a polarizing set of d functions on the non-hydrogen atoms.[21] Auxiliary basis sets used to expand the electron density in the calculations were chosen to match the orbital basis. Electronic energies and properties were calculated at the optimized geometries using the B3LYP functional.[19,23] In this case the same basis sets were used. The self-consistent field calculations were tightly converged (1×10^{-8} E_h in energy, 1×10^{-7} E_h in the density charge, and 1×10^{-7} in the maximum element of the DIIS[24] error vector). The geometry search for all complexes was carried out in redundant internal coordinates without imposing geometry constraints. Corresponding[25] and quasi-restricted[26] orbitals and density plots were obtained using Molekel.[27] We used the broken symmetry (BS) approach to describe our computational results for **1**, **2**, **4**, and $Cr(pdt)_3$.[4,28] We adopted the following notation: the given system was divided into two fragments. The notation BS(*m*,*n*) refers then to a broken symmetry state with *m* unpaired α-spin electrons essentially on fragment 1 and *n* unpaired *β*-spin electrons localized on fragment 2. In most cases, fragments 1 and 2 correspond to the metal and the ligands, respectively. In this notation the standard high-spin, open-shell solution is written as BS($m + n$,0). The BS(*m*,*n*) notation refers to the initial guess to the wave function. The variational process does, however, have the freedom to converge to a solution of the form BS($m - n$,0) in which effectively the n *β*-spin electrons pair up with $n < m$ α-spin electrons on the partner fragment. Such a solution is then a standard $M_S \cong (m - n)/2$ spin-unrestricted Kohn−Sham solution. As explained elsewhere,[25] the nature of the solution is investigated from the corresponding orbital transformation (COT) which, from the corresponding orbital overlaps, displays whether the system should be described as a spin-coupled or a closed-shell solution.

Time-dependent (TD-DFT) calculations of the metal and sulfur K-pre-edges were conducted as previously described.[29,30] For all complexes, the BP86 functional was used in conjunction with the fully uncontracted CP(PPP) basis set for the metal,[31] TZVP for the sulfur and SV(P) for the remaining atoms for a single point, spin unrestricted ground state DFT calculation starting from the optimized coordinates. TD-DFT calculations[32] were then performed allowing only for transitions from the metal (Cr and Mn) 1s orbital.[30,33] For the S K-edge spectra, the six sulfur 1s orbitals were localized and the TD-DFT equations were solved for each sulfur atom, excluding all but excitations originating from the 1s orbital.[29,34,35] The absolute calculated transition energies are consistently underestimated because of shortcomings in the ability of DFT to model potentials near the nucleus. This results in the deep 1s core orbitals being too high in energy relative to the valence, thus requiring a constant shift for a given absorber.[29,30] It was established that shifts of 154.9 eV for Cr K-edge, 169.4 eV for Mn K-edge, and 77.0 eV for S K-edge are required for this regime of basis sets and applied to the transition energies. Plots were obtained using "orca_mapspc" with a line

(19) Becke, A. D. *Phys. Rev. A* **1988**, *38*, 3098.
(20) Perdew, J. P. *Phys. Rev. B* **1986**, *33*, 8822.
(21) Schäfer, A.; Horn, H.; Ahlrichs, R. *J. Chem. Phys.* **1992**, *97*, 2571.
(22) Schäfer, A.; Huber, C.; Ahlrichs, R. *J. Chem. Phys.* **1994**, *100*, 5829.
(23) (a) Becke, A. D. *J. Chem. Phys.* **1993**, *98*, 5648. (b) Lee, C. T.; Yang, W. T.; Parr, R. G. *Phys. Rev. B* **1988**, *37*, 785.
(24) (a) Pulay, P. *Chem. Phys. Lett.* **1980**, *73*, 393. (b) Pulay, P. *J. Comput. Chem.* **1992**, *3*, 556.
(25) Neese, F. *J. Phys. Chem. Solids* **2004**, *65*, 781.
(26) Schöneboon, J. C.; Neese, F.; Thiele, W. *J. Am. Chem. Soc.* **2005**, *127*, 5840.
(27) *Molekel, Advanced Interactive 3D-Graphics for Molecular Sciences*, Swiss National Supercomputing Center. http://www.cscs.ch/molkel.
(28) (a) Noodleman, L. *J. Chem. Phys.* **1981**, *74*, 5737. (b) Noodleman, L.; Case, D. A.; Aizman, A. *J. Am. Chem. Soc.* **1988**, *110*, 1001. (c) Noodleman, L.; Davidson, E. R. *Chem. Phys.* **1986**, *109*, 131. (d) Noodleman, L.; Norman, J. G.; Osborne, J. H.; Aizman, A.; Case, D. A. *J. Am. Chem. Soc.* **1985**, *107*, 3418. (e) Noodleman, L.; Peng, C. Y.; Case, D. A.; Monesca, J. M. *Coord. Chem. Rev.* **1995**, *144*, 199.
(29) DeBeer George, S.; Petrenko, T.; Neese, F. *Inorg. Chim. Acta* **2008**, *361*, 965.
(30) DeBeer George, S.; Petrenko, T.; Neese, F. *J. Phys. Chem. A* **2008**, *112*, 12936.
(31) Neese, F. *Inorg. Chim. Acta* **2002**, *337*, 181.
(32) Neese, F.; Olbrich, G. *Chem. Phys. Lett.* **2002**, *362*, 170.
(33) (a) Berry, J. F.; DeBeer George, S.; Neese, F. *Phys. Chem. Chem. Phys.* **2008**, *10*, 4361. (b) Yano, J.; Robblee, J.; Pushkar, Y.; Marcus, M. A.; Bendix, J.; Workman, J. M.; Collins, T. J.; Solomon, E. I.; DeBeer George, S.; Yachandra, V. K. *J. Am. Chem. Soc.* **2007**, *129*, 12989.
(34) Ray, K.; DeBeer George, S.; Solomon, E. I.; Wieghardt, K.; Neese, F. *Chem.—Eur. J.* **2007**, *13*, 2783.
(35) Kapre, R. R.; Ray, K.; Sylvestre, I.; Weyhermüller, T.; DeBeer George, S.; Neese, F.; Wieghardt, K. *Inorg. Chem.* **2006**, *45*, 3499.

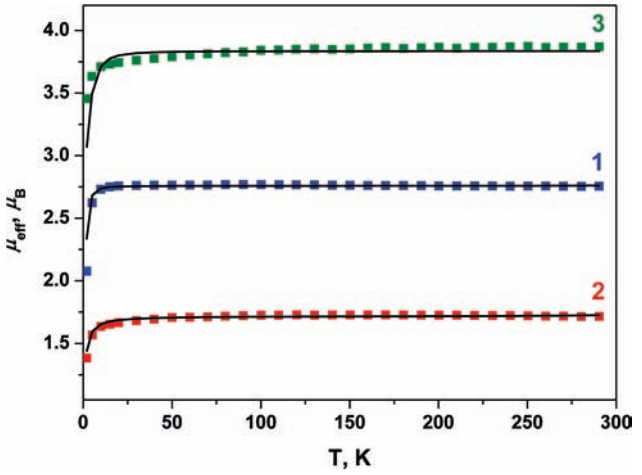

Figure 1. Temperature-dependence of the magnetic moment, μ_{eff}, μ_B, of powdered samples of **1**, **2**, and **3**. The filled squares represent the experimental data, whereas the solid lines represent simulations (see text).

broading of 1.0 eV for metal K-edges and 0.8 eV for S K-edges. Despite the inherent restrictions in describing open-shell systems with a single determinantal reference wave function,[34,36] we have found this method is quite effective at predicting the energy and relative intensities for transitions originating from the Cr or S 1s orbital for **1**, **2**, **4**, neutral octahedral $Cr(pdt)_3$, and the $[Cr\text{-}(tbbdt)_3]^z$ ($z = 0, 1-, 2-$) series.

Results

Syntheses and Characterization. From the reaction mixture of 3 equiv of the ligand 3,6-dichlorobenzene-1,2-dithiol, $H_2(Cl_2\text{-bdt})$, 1 equiv of $[Cr^{III}Cl_3(thf)_3]$, and 6 equiv of triethylamine in tetrahydrofuran (thf) in the presence of a small amount of air were obtained, upon addition of $[N(n\text{-}Bu)_4]Br$, dark green microcrystals of $[N(n\text{-}Bu)_4]_2[Cr(Cl_2\text{-bdt})_3]$ (**1**) in good yields. From magnetic susceptibility measurements (4−300 K) a temperature-independent magnetic moment of 2.78 μ_B (10−300 K) as shown in Figure 1 was established.

This is indicative of an $S = 1$ ground state in excellent agreement with the corresponding dianion $[Cr(mnt)_3]^{2-}$ (**4**), prepared as described using phosphonium rather than arsonium countercation.[1,6] Oxidation of the arsonium salt of **1** with 1 equiv of ferrocenium hexafluorophosphate in CH_2Cl_2 yielded violet microcrystals of $[AsPh_4][Cr(Cl_2\text{-bdt})_3]$ (**2**). Magnetic susceptibility measurements yielded a temperature-independent magnetic moment of 1.73 μ_B indicative of an $S = {}^1/_2$ ground state. The X-band EPR spectrum of **2** in CH_2Cl_2/toluene solution displays an axial signal at 10 K with $g_\perp = 2.006$ and $g_\parallel = 2.010$ and hyperfine of $A \approx 16 \times 10^{-4}$ cm^{-1} because of the coupling of the ^{53}Cr ($I = {}^3/_2$, 9.54% natural abundance) isotope (Supporting Information, Figure S4). A near identical spectrum was recorded for electrochemically generated $[Cr(mnt)_3]^{1-}$ (Supporting Information, Figure S5) and spectra of other monoanions such as $[Cr(tfd)_3]^{1-}$,[1] $[Cr\text{-}(Cl_4\text{-bdt})_3]^{1-}$.[3] An axial signal with $g_\perp = 1.9947$ and $g_\parallel = 2.0074$ was exhibited by $[Cr(tbbdt)_3]^{1-}$.[4] EPR spectroscopic results are summarized in Table 2.

Reduction of **1** by 1 equiv of sodium metal under anaerobic conditions in thf yielded light green microcrystalline $[N(n\text{-}Bu)_4]_3[Cr(Cl_2\text{-bdt})_3]\cdot thf$ (**3**). A temperature-independent magnetic moment of 3.8 μ_B (50−300 K) (Figure 1) is indicative of an $S = {}^3/_2$ ground state, as has been shown to be the case for the analogous $[PPh_4]_3[Cr(mnt)_3]$ (**5**).[1,6] The decrease of the magnetic moment of **3** at temperatures below 50 K has been successfully modeled by a zero-field splitting parameter $D = -3.3 \pm 1$ cm^{-1} determined from EPR. Weak intermolecular antiferromagnetic interactions may also be present. The X-band EPR spectrum of **5** in CH_2Cl_2/dmf at 10 K shown in Figure 2 (top) is typical of a Cr(III) $S = {}^3/_2$ ground state. The spectrum possesses a dominating derivative signal at $g_{eff,\perp} \approx 4$ and a negative line at $g_{eff,\parallel} \approx 2$, which are due to the $m_s = \pm{}^1/_2$ Kramer's doublet with large zero-field splitting ($D > h\nu$). A sharp resolved peak at $g_{eff} \approx 6$ originates from the $m_s = \pm{}^3/_2$ Kramer's doublet, which is obscured in the $g_{eff,\perp}$ in the spectrum of **3** (Supporting Information, Figure S6). A spectrum recorded at 4 K shows an increase in the intensity of the $g_{eff} \approx 6$ peak and infers that the $|{}^3/_2, \pm{}^3/_2\rangle$ doublet is the ground state and, thus, D is negative (inset in Figure 2, top).

The spectra of **5** recorded at 4 and 10 K were readily simulated by using a full-spin Hamiltonian routine for $S = {}^3/_2$ with the following parameters: $D = -1.6$ cm^{-1}; $E/D = 0.073$; $g = (1.97, 1.97, 1.98)$. The poorly resolved spectra of **3** at 4 and 10 K were simulated with the following parameters: $D = -3.3 \pm 1$ cm^{-1}; $E/D = 0.08$; $g = (1.98, 1.98, 1.96)$. For both samples, the broad lines were reproduced by adopting a Gaussian distribution of E/D with a half-width $\sigma = 0.042$.

The reaction of 1 equiv of $MnCl_2\cdot 4H_2O$ with 3 equiv of $H_2(Cl_2\text{-bdt})$ in ethanol in the presence of air produced a magenta-colored solution from which upon addition of $[NEt_4]Br$ magenta microcrystals of $[NEt_4]_2[Mn(Cl_2\text{-bdt})_3]$ were obtained. Recrystallization from a CH_2Cl_2/EtOH mixture produced single crystals of $[NEt_4]_2[Mn(Cl_2\text{-bdt})_3]\cdot CH_2Cl_2$ (**6**). Mint green $[PPh_4]_2[Mn(mnt)_3]$ ($S = {}^3/_2$) (**7**) has been prepared as described in ref 5. From magnetic susceptibility measurements a temperature-independent magnetic moment (20−300 K) of $\mu_{eff} = 3.83$ μ_B is indicative of an $S = {}^3/_2$ ground state for **6** (Supporting Information, Figure S1) with a similar result for **7** (4.18 μ_B, 50−300 K, Supporting Information, Figure S2). The X-band EPR spectra of $[Mn^{IV}(Cl_2\text{-bdt})_3]^{2-}$ in **6** (Supporting Information, Figure S7) and $[Mn^{IV}(mnt)_3]^{2-}$ in **7** (Figure 2) and the monocation $[Mn^{IV}(dtc)_3]^+$ in **9** (Supporting Information, Figure S8) are very similar. The X-band EPR spectrum of **7** in a thf solution at 10 K has characteristics identical to those described for isoelectronic **5** (Cr(III), $S = {}^3/_2$), with the addition of nicely resolved, 6-line hyperfine splittings from interactions with the ^{55}Mn nuclei

Table 2. Simulated EPR Spin Hamiltonian Parameters g, A ($\times 10^{-4}$ cm^{-1}), D (cm^{-1}) and E/D for $S = {}^1/_2$ and $S = {}^3/_2$ Complexes

	g_x	g_y	g_z	A_{xx}	A_{yy}	A_{zz}	D	E/D
2	2.006	2.006	2.010	18	18	7		
$[Cr(mnt)_3]^{1-}$	1.993	1.995	2.001	20	20	8		
3	1.980	1.980	1.960				−3.3	0.080
5	1.970	1.970	1.980				−1.6	0.073
6	2.020	2.020	1.970	190[a]	190[a]	66[a]	−1.6	0
7	2.039	2.039	2.010	20	20	55	−1.3	0.071
9	2.020	2.020	1.960	198[a]	198[a]	[b]	−1.27	0.150

[a] Obtained directly from the experimental spectrum. [b] Not resolved.

(36) Herebian, D.; Wieghardt, K.; Neese, F. *J. Am. Chem. Soc.* **2005**, *125*, 10997.

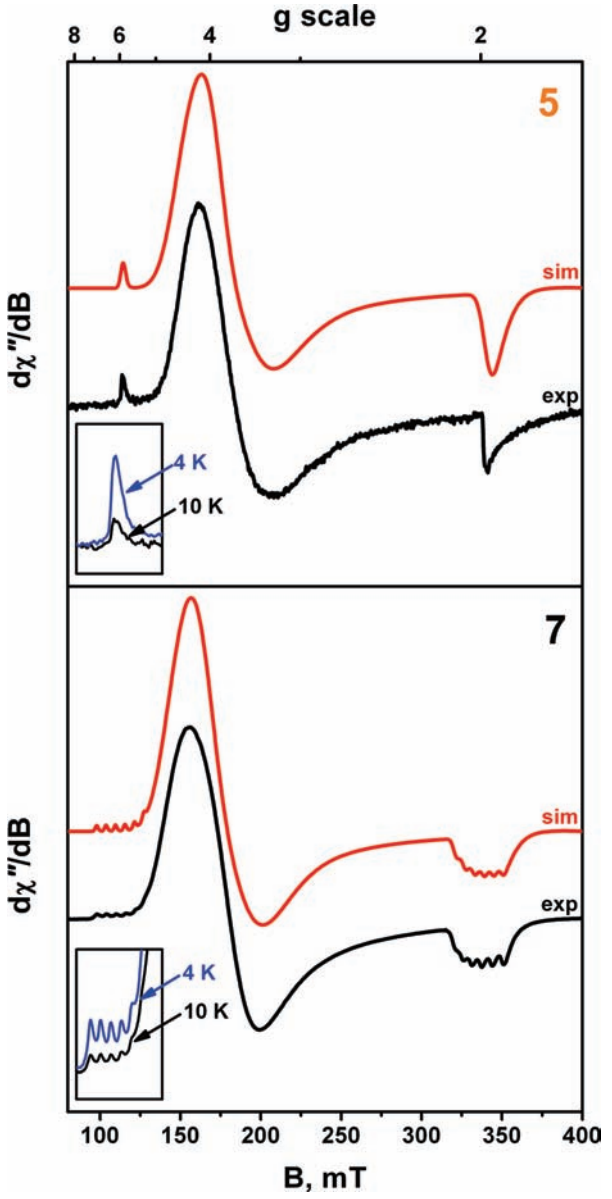

Figure 2. Representative X-band EPR spectra of Cr and Mn $S = {}^3/_2$ complexes. Top: CH_2Cl_2/DMF solution of **5** at 10 K (conditions: frequency 9.43 GHz; power 0.20 mW; modulation 1.0 mT). Bottom: **7** recorded in thf at 10 K (conditions: frequency 9.43 GHz; power 0.63 mW; modulation 1.0 mT). Simulations are shown in red, and parameters are given in the text. Insets show intensity of the resolved peak at $g_{eff} = 6$ from the excited $m_s = \pm{}^3/_2$ Kramer's doublet. The greater intensity in the 4 K spectrum indicates a negative zero-field splitting for these complexes.

at $g_{eff,z}$. For **7**, the $g_{eff} \approx 6$ is well resolved, while it is buried in the $g_{eff} \approx 4$ signal in **6** and **9**. Variable temperature measurements reveal D is negative (insets, Figure 2), and simulation of the 5 and 10 K spectra of **7** was achieved with $D = -1.3\ cm^{-1}$, $E/D = 0.071$, and $g = (2.039, 2.039, 2.010)$. The experimental linewidth was realized using a Gaussian distribution of the rhombicity with $\sigma = 0.040$. The corresponding spin-Hamiltonian parameters of simulations with first-order hyperfine couplings are given in Table 2.

Furthermore, we prepared two manganese complexes with the relatively redox inert dithiocarbamate(1−) ligand, namely, $[Mn^{III}(dtc)_3]$ (**8**) and $[Mn^{IV}(dtc)_3](BF_4)$ (**9**) according to ref 12e. These serve as important calibrants in XAS studies. Complex **8** displays a temperature-independent

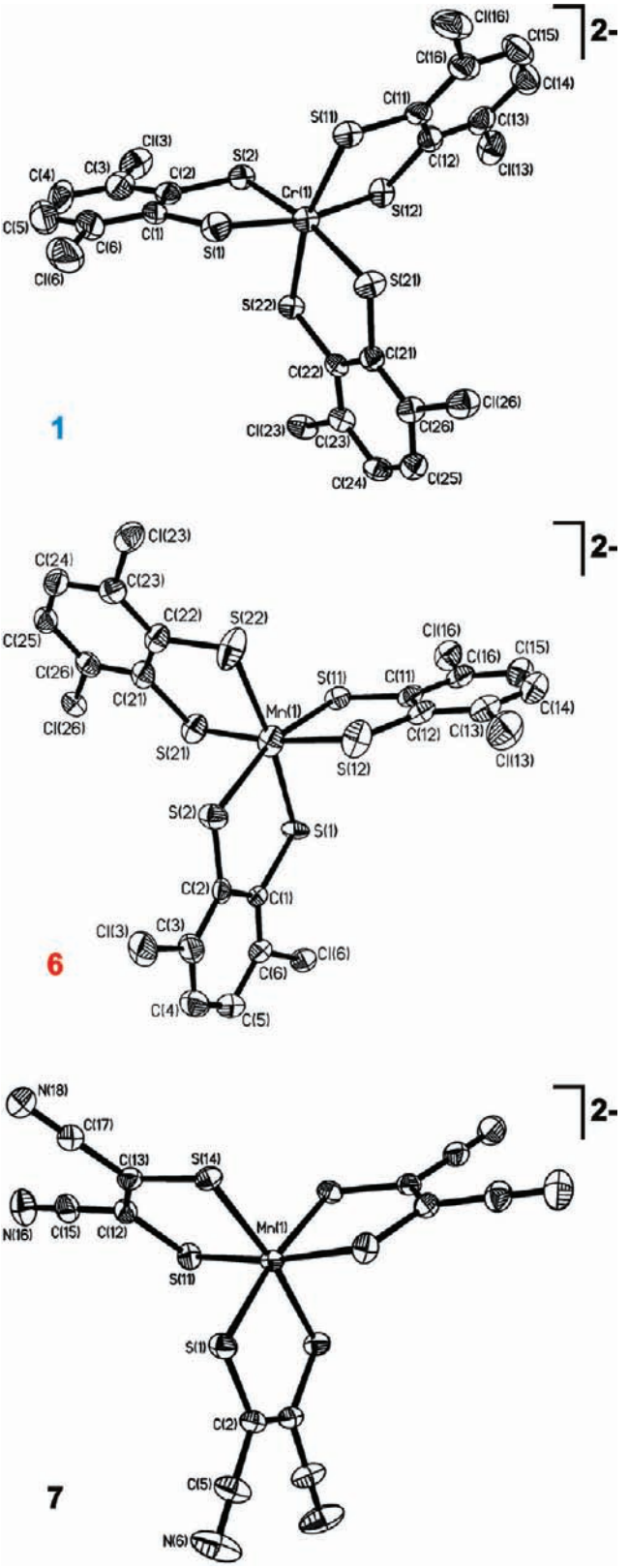

Figure 3. Structure of the dianion in crystals of **1** (top), of the dianion in crystals of **6**, and the dianion in crystals of **7**.

(20−300 K) magnetic moment of 4.95 μ_B in agreement with the previously reported $S = 2$ ground state (Supporting Information, Figure S3). On the other hand, **9** exhibits a temperature-independent magnetic moment of 3.92 μ_B (60−300 K) which is in accord with an $S = {}^3/_2$ ground

Table 3. Selected Bond Distances (Å) and Angles (deg) of the Anions in Crystals of **1**, **6**, and **7**

		Complex **1**			
Cr(1)−S(1)	2.313(2)	Cr(1)−S(11)	2.350(2)	Cr(1)−S(21)	2.330(2)
Cr(1)−S(2)	2.317(2)	Cr(1)−S(12)	2.358(2)	Cr(1)−S(22)	2.325(2)
S(1)−C(1)	1.739(6)	S(11)−C(11)	1.746(6)	S(21)−C(21)	1.744(5)
S(2)−C(2)	1.739(6)	S(12)−C(12)	1.742(6)	S(22)−C(22)	1.740(5)
C(1)−C(2)	1.396(8)	C(11)−C(12)	1.400(8)	C(21)−C(22)	1.422(7)
C(1)−C(6)	1.414(9)	C(11)−C(16)	1.412(8)	C(21)−C(26)	1.382(7)
C(2)−C(3)	1.403(9)	C(12)−C(13)	1.396(8)	C(22)−C(23)	1.392(7)
C(3)−C(4)	1.374(10)	C(13)−C(14)	1.386(10)	C(23)−C(24)	1.382(8)
C(4)−C(5)	1.395(12)	C(14)−C(15)	1.384(10)	C(24)−C(25)	1.392(8)
C(5)−C(6)	1.371(11)	C(15)−C(16)	1.381(10)	C(25)−C(26)	1.384(8)
S(1)−Cr(1)−S(2)	86.64(6)	S(11)−Cr(1)−S(12)	84.97(6)	S(21)−Cr(1)−S(22)	85.70(6)
S(1)−Cr(1)−S(12)	167.83(7)	S(11)−Cr(1)−S(22)	165.83(7)	S(2)−Cr(1)−S(21)	169.59(6)
		Complex **6**			
Mn(1)−S(1)	2.382(5)	Mn(1)−S(11)	2.328(1)	Mn(1)−S(21)	2.322(2)
Mn(1)−S(2)	2.399(3)	Mn(1)−S(12)	2.336(2)	Mn(1)−S(22)	2.315(2)
S(1)−C(1)	1.805(9)	S(11)−C(11)	1.756(6)	S(21)−C(21)	1.762(5)
S(2)−C(2)	1.728(12)	S(12)−C(12)	1.748(6)	S(22)−C(22)	1.762(6)
C(21)−C(22)	1.409(8)	C(22)−C(23)	1.405(7)	C(24)−C(25)	1.377(8)
C(21)−C(26)	1.399(8)	C(23)−C(24)	1.387(8)	C(25)−C(26)	1.386(8)
S(1)−Mn(1)−S(2)	82.30(14)	S(11)−Mn(1)−S(12)	86.59(6)	S(21)−Mn(1)−S(22)	86.81(6)
S(1)−Mn(1)−S(22)	172.3(3)	S(2)−Mn(1)−S(11)	163.60(9)	S(12)−Mn(1)−S(21)	172.12(7)
		Complex **7**			
Mn(1)−S(1)	2.3256(4)	Mn(1)−S(11)	2.3345(4)	Mn(1)−S(14)	2.3240(4)
S(1)−C(2)	1.745(1)	S(11)−C(12)	1.747(2)	S(14)−C(13)	1.748(2)
C(2)−C(2)′	1.358(3)	C(12)−C(13)	1.360(2)	C(13)−C(17)	1.440(2)
C(2)−C(5)	1.437(2)	C(12)−C(15)	1.436(2)	C(17)−N(18)	1.153(2)
C(5)−N(6)	1.153(2)	C(15)−N(16)	1.153(2)		
S(1)−Mn(1)−S(1)′	87.76(2)	S(11)−Mn(1)−S(14)	87.66(2)	S(11)′−Mn(1)−S(14)	87.33(2)
S(1)′−Mn(1)−S(14)	171.83(2)	S(1)′−Mn(1)−S(14)′	85.92(1)	S(14)−Mn(1)−S(14)′	100.82(2)

state (Supporting Information, Figure S3). Note that the EPR spectrum of **9** with a signal at $g \sim 2$ reported in ref 12b is due to a Mn(II) impurity, readily differentiated from a true $S = {}^3/_2$ signal because of its crossing point in the first-derivative spectrum. Complex **9** is light sensitive, and we have observed decomposition to Mn(II) in thf, though it is quite stable in CH_2Cl_2. The true X-band EPR spectrum, recorded in CH_2Cl_2/toluene, is shown in Supporting Information, Figure S8, and the data are given in Table 2.

The crystal structures of **1**, **6**, and **7** have been determined by single crystal X-ray crystallography at 100 K. Figure 3 shows the structures of (a) the dianion $[Cr(Cl_2\text{-bdt})_3]^{2-}$ in crystals of **1**, (b) the dianion $[Mn(Cl_2\text{-bdt})_3]^{2-}$ in crystals of **6**, and (c) the dianion $[Mn(mnt)_3]^{2-}$ in crystals of **7**. Table 3 summarizes selected bond distances and angles. It is worth noting that the intraligand bond distances of the mnt^{2-} in **7** are very similar to the isoelectronic **5** and its one-electron oxidized **4**.[7] Monoanionic $[Ni(mnt)_2]^{1-}$ possesses one radical ligand while the dianion, $[Ni(mnt)_2]^{2-}$ has two closed-shell ligands, and thus both have a central Ni(II) ion.[37] The intraligand bond distances for these two anions are quite similar, highlighting the difficulty in assigning oxidation levels in the ligand,[38] a consequence of the extensive conjugation throughout the mnt^{2-} unit.

The MS_6 polyhedron in all three dianions is best described as distorted octahedral. The twist angle Θ is the chelate projection angle which is 60° in a regular octahedron and 0° in a trigonal prism. The following angles, α, α′, and α″ are defined as the dihedral angle between an MS_2 plane and the corresponding S_2C_2 plane of each bidentate ligand (Scheme 3). Table 4 summarizes these angles for the structurally characterized tris(dithiolene)metal complexes of Cr and Mn.

Irrespective of the nature of the central metal ion (Cr or Mn) and irrespective of the actual charge of the anion (1−, 2−, or 3−) the average twist angle Θ is always > 39° indicating substantial distortion toward an octahedron.[39] We take this as a structural indication that complexes **1**−**7** contain a metal ion with a d^n electron configuration with $n > 2$ (probably 3). It has been suggested that trigonal prismatic tris(dithiolene)metal complexes are stable only with a d^n configuration where $n = 0$, 1, or 2.[9] The av. folding angle α is smaller than 14° in all complexes of chromium and manganese considered here.

Electrochemistry. Supporting Information, Figure S9 shows the cyclic voltammogram (cv) of **1** in CH_2Cl_2

(37) Sarangi, R.; DeBeer George, S.; Jackson Rudd, D.; Szilagyi, R. K.; Ribas, X.; Rovira, C.; Almeida, M.; Hodgson, K. O.; Hedman, B.; Solomon, E. I. *J. Am. Chem. Soc.* **2007**, *129*, 2316.

(38) (a) Mahadevan, C.; Seshasayee, M.; Murthy, B. V. R.; Kuppusamy, P.; Manoharan, P. T. *Acta Crystallogr.* **1983**, *C39*, 1335. (b) Mahadevan, C.; Seshasayee, M.; Radha, A.; Manoharan, P. T. *Acta Crystallogr.* **1984**, *C40*, 2032.

(39) The magnitude of the twist angle Θ is a function of the bite angle of a bidentate ligand. The normalized bite angle is defined as the distance between the donor atoms of the chelate divided by the metal-ligand bond length (Kepert, D. L. *Prog. Inorg. Chem.* **1977**, *23*, 1). From this value, an octahedral limit (Θ_{lim}) can be determined for any given complex. Here, Θ_{lim} for **8** and **9** are 40.2° and 39.0°, respectively. Much larger values of ∼55° are calculated for the dithiolene complexes. We can observe that **8** and **9** achieve this value experimentally, while the dithiolene complexes are 3−16° short of their limit which implies additional interactions cause further distortion away from octahedral.

Scheme 3. Twist Angle Θ and Folding Angles α, α′, α″

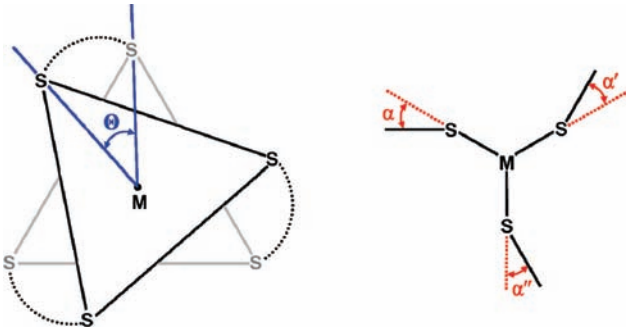

Table 4. Twist Angles Θ (deg) and Folding Angles α (deg) in [M(dithiolene)$_3$] (M = Cr, Mn) Complexes

complex	Θ	α	α′	α″	ref
1	49.7, 42.5, 44.5	16.5	4.9	10.7	this work
$[Cr(tbbdt)_3]^{1-}$	46.0, 37.7, 33.7	12.9	23.6	6.5	4
4	41.7, 47.2, 47.2	0	7.2	7.2	7
5	51.8, 52.8, 50.1	12.5	6.7	8.2	7
6	45.0, 47.8, 51.7	6.7	3.1	15.5	this work
7	49.2, 51.4, 49.2	12.0	11.9	0.03	this work
$[Mn(bdt)_3]^{2-}$	41.1, 39.2, 41.1	3.4	3.2	0.9	11
8	39.8, 35.4, 45.0	9.6	5.2	3.8	12a, 13
9[a]	39.6, 39.4, 38.0	3.0	3.4	9.7	12d, 12f

[a] Data are taken from the structure of tris(pentamethylenedithiocarbamato)manganese(IV) perchlorate.

Table 5. Redox Potentials (V) of Complexes vs Fc^+/Fc

complex	$E^1_{1/2}$[a]	$E^2_{1/2}$[b]	$E^3_{1/2}$[c]
1	+0.19 irr	−0.36 r	−0.85 r
$[Cr(Cl_4\text{-}bdt)_3]^{1-}$[d]	+0.47 irr	−0.27 r	−0.74 r
$[Cr(tbbdt)_3]^{1-}$[e]	−0.25 r	−0.94 r	−1.57 r
$[Cr(tfd)_3]^{0}$[f]	+0.64 r	−0.10 r	
4	+0.85 irr	+0.29 r	−0.34 r
6		−0.12 irr	−1.53 r
$[Mn(Cl_4\text{-}bdt)_3]^{2-}$[d]		+0.02 r	−1.30 r
7			−0.70 r

[a] 0/1− couple. [b] 1−/2− couple. [c] 2−/3− couple (r = reversible; irr = irreversible). [d] Ref 3. The original data recorded in dichloromethane were referenced vs an aqueous standard calomel electrode (SCE) with LiCl; here they are converted by adding −0.38 eV. [e] Ref 4. [f] Ref 1. The original data recorded in dmso were referenced vs SCE with NaCl; here they are converted by adding −0.50 V.

solution containing 0.10 M $[N(n\text{-}Bu)_4]PF_6$ supporting electrolyte at 22 °C at a glassy carbon working electrode. All redox potentials (Table 5) are referenced versus the ferrocenium/ferrocene couple (Fc^+/Fc). The cv of **1** displays two successive, fully reversible one-electron transfer waves ($E^2_{1/2}$ and $E^3_{1/2}$) and an irreversible oxidation peak at $E_{p,a} = 0.19$ V.

The latter peak is reversible for the series $[Cr(tbbdt)_3]^z$ ($z = 0, 1-, 2-, 3-$). For $[Cr(Cl_4\text{-}bdt)_3]^z$ ($z = 0, 1-, 2-, 3-$) there are also three fully reversible one-electron transfer waves reported.[3] For $[Cr(mnt)_3]^z$ ($z = 1-, 2-, 3-$) complexes only two reversible waves are seen, as observed previously.[6] It is of interest to note the values for $E^{1-3}_{1/2}$ for each individual series vary significantly with the nature of the dithiolene ligand. Thus, complexes containing tetrachlorobenzene-1,2-dithiolate ligands are much more difficult to oxidize than their 3,5-di-*tert*-butylbenzene-1,2-dithiolate analogues, and $(Cl_2\text{-}bdt)^{2-}$ is intermediate between these two. Thus, the redox potential $E^3_{1/2}$, for the oxidation of the trianion $[Cr(Cl_4\text{-}bdt)_3]^{3-}$ to the corresponding dianionic species is more positive by 0.11 V than the corresponding value for the couple $[Cr(Cl_2\text{-}bdt)_3]^{3-/2-}$ and 0.72 V more than the couple $[Cr(tbbdt)_3]^{3-/2-}$. The same order holds for the 2−/1− couples of these three series. We interpret this behavior as an indication that these redox processes are ligand-centered rather than metal-centered and do not involve high-valent Cr(IV), Cr(V), or Cr(VI). Interestingly, $[Cr(mnt)_3]^{1-}$ is the most difficult species to oxidize.[1,6] For the tris(dithiolene)manganese complexes $[Mn(Cl_2\text{-}bdt)_3]^{2-}$ and $[Mn(Cl_4\text{-}bdt)_3]^{2-}$, and $[Mn(mnt)_3]^{2-}$ the 3−/2− couple is reversible,[1,3,6] where the latter species possesses the most positive redox potential. In all of these instances the one-electron reduction is metal-centered: the central Mn(IV) ion ($S_{Mn} = {}^3/_2$) in the dianions is reduced to the corresponding high-spin manganese(III) ion ($S_{Mn} = 2$).

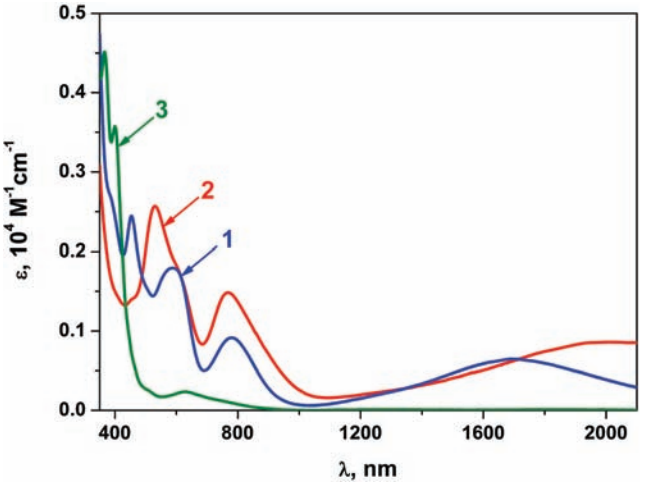

Figure 4. Electronic spectra of **1**, **2**, and **3** recorded in CH_2Cl_2 at room temperature.

Electronic Spectra. The electronic spectra of complexes **1**−**3** have been recorded in CH_2Cl_2 solution; they are shown in Figure 4, and the electronic absorption data summarized in Table 6. These spectra are very similar to those reported previously for the series $[Cr(tbbdt)_3]^z$ ($z = 0, 1-, 2-, 3-$).[4] The spectra of the trianions in **3**, **5**, and $[Cr(tbbdt)_3]^{3-}$ display two or three d-d transitions in the visible region of comparatively low intensity, which is quite typical for distorted octahedral chromium(III) complexes. The spectra of the mono- and dianions in **2**, **1**, and **4**, exhibit a typical ligand-to-ligand charge transfer (LLCT) band in the near-infrared at 2021 nm ($\varepsilon = 860$ M^{-1} cm^{-1}), 1688(650), and 2071(1800), respectively. This transition is proposed to be an intervalence CT (IVCT) band between an *S*,*S*-coordinated, closed-shell ligand dianion and a monoanionic π radical ligand $((L^{\bullet})^{1-}/L^{2-})$.[40] In $[Cr(tbbdt)_3]^{1-/2-}$ these bands have been observed at 1750(3000) and 1720(2500) nm, respectively.[4] It is absent in $[Cr(mnt)_3]^{3-}$ and in the neutral complexes $[Cr(pdt)_3]^0$ and $[Cr(tbbdt)_3]^0$ where three π radical monoanions are *S*,*S*-coordinated to a central Cr(III) ion.[4,9,10] As noticed before the electronic spectra of these tris(dithiolene)chromium complexes resemble

(40) Chang, H.-C.; Myasaka, H.; Kitagawa, S. *Inorg. Chem.* **2001**, *40*, 146.

Table 6. Electronic Spectra of Complexes in CH_2Cl_2 Solutions

complex	λ_{max}, nm (ε, 10^4 M^{-1} cm^{-1})
1	454 (0.26), 590 (0.17), 780 (0.08), 1695 (0.06)
2	530 (0.35), 620 sh (0.23), 770 (0.14), 1960 (0.07)
3	400 (0.39), 630 (0.05)
4	481 (0.77), 571 sh (0.39), 686 (0.47), 1005 (0.03), 2071 (0.18)
5	425 (0.98), 470 (0.66), 560 (0.22), 668 (0.11)
6	342 (0.42), 374 (0.48), 511 (0.12), 571 (0.09), 714 (0.09)
7	596 sh (0.45), 633 (0.55), 834 (0.48)
$[Cr(pdt)_3]^{0a}$	581(2.7), 686(0.3)
$[Cr(tbbdt)_3]^{0b}$	590(2.0), 700(0.9)

[a] Refs 2 and 9; measured in chloroform. [b] Ref 4; electrochemically generated.

closely those reported previously for the corresponding tris(dioxolene)chromium complexes.[4,41]

X-ray Absorption Spectroscopy. Cr and Mn K-edge XAS. Cr and Mn K-edge XAS data for complexes **1**−**5** and **6**− **9** are shown in Figures 5 and 6, respectively. Table 7 summarizes the 1s → 3d pre-edge energies (transition A) and the rising edge energies for **1**−**9** (transition C). In some cases, an additional transition is observed (B), which may be attributed to a formally two electron 1s to 4p + LMCT shakedown transition[37] or could reflect a transition to an unoccupied ligand orbital with significant metal 4p character. Pre-edge energies are dominated by ligand field contributions. Since for a given ligand set the ligand field will increase with increasing oxidation state, the pre-edge energy provides a useful marker for oxidation state. The Cr pre-edge energies of the electron-transfer series **1**, **2**, and **3** are identical, within experimental error, at 5990.1 ± 0.2 eV. As a ~1 eV increase in energy is expected per unit of oxidation, these data indicate that the Cr oxidation state remains the same across the series **2**, **1**, and **3**, namely Cr(III). The same holds true for the rising edge energies which provide a measure of the effective nuclear charge, Z_{eff}.

Interestingly, the pre-edge energy of the monoanion $[Cr(tbbdt)_3]^{1-}$ has also been reported at 5989.7 eV indicating the presence of a Cr(III) ion.[4] There are two pre-edge peaks for complexes **4** and **5** observed in the narrow range 5990.3−5992.4 eV (average 5990.8 eV for **4** and 5991.4 eV for **5**), with additional shoulder at ~5989.6 eV for **4**. This as an indication that oxidation of **5** to **4** does not involve a change of the chromium oxidation state which is again +III (d^3) in both cases.

Similarly, complexes **6**, **7**, and **9** display the Mn pre-edge energy invariably at ~6540.3 eV which indicates the presence of a central Mn(IV) ion in an octahedral MnS_6 polyhedron in each species. For the neutral $[Mn(dtc)_3]^0$ species **8** the energy of the pre-edge is ~0.3 eV lower in energy. The origin of this small difference is elaborated by

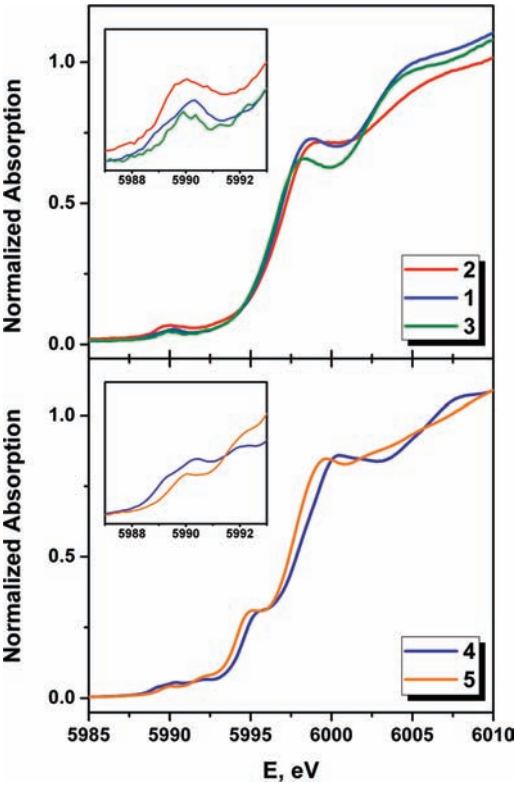

Figure 5. Comparison of the normalized Cr K-edge data for the dianion in **1**, the monoanion in **2**, and the trianion in **3**. The Cr K-edge data for the dianion in **4** and the trianion in **5** are given at the bottom. The insets show expansions of the pre-edge region.

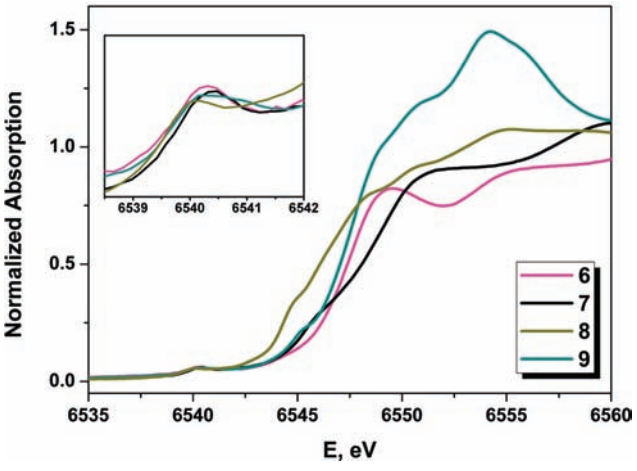

Figure 6. Comparison of the normalized Mn K-edge data for complexes **6**−**9**. The inset shows an expansion of the pre-edge region.

TD-DFT (vide infra). However, since the rising-edge energy at 6545.9 eV is ~2.3 eV lower in energy than that of **6**, **7**, and **9**, we take this as clear evidence that the one-electron reduction of cationic **9** to neutral **8** is metal-centered (Mn(IV), d^3 → Mn(III), high-spin d^4).

Sulfur K-edge XAS. Figure 7 (top) shows a comparison of the experimental S K-edge spectra of the mono-, di-, and trianionic species in crystals of **2**, **1**, and **3**; the pseudo-Voigt deconvoluted spectra of **4** and **5** are shown in Figure 8. The results of the analysis of the pre-edge and near-edge peak energies are given in Table 7 and in the Supporting Information. The spectra of the mono-anion in **2** and of the dianions in **1** and **4** all display

(41) (a) Pierpont, C. G. *Coord. Chem. Rev.* **2001**, *216*−*217*, 99. (b) Pierpont, C. G. *Coord. Chem. Rev.* **2001**, *219*−*221*, 415. (c) Pierpont, C. G.; Buchanan, R. M. *Coord. Chem. Rev.* **1981**, *38*, 45. (d) Pierpont, C. G.; Lange, C. W. *Prog. Inorg. Chem.* **1994**, *41*, 331. (e) Isied, S. S.; Kuo, G.; Raymond, K. N. *J. Am. Chem. Soc.* **1976**, *98*, 1763. (f) Raymond, K. N.; Isied, S. S.; Brown, L. D.; Fronczek, F. R.; Nibert, J. H. *J. Am. Chem. Soc.* **1976**, *98*, 1767. (g) Sofen, S. R.; Ware, D. C.; Cooper, S. R.; Raymond, K. N. *Inorg. Chem.* **1979**, *18*, 1736. (h) Buchanan, R. M.; Clafin, J.; Pierpont, C. G. *Inorg. Chem.* **1983**, *22*, 2552. (i) Pierpont, C. G.; Downs, H. H. *J. Am. Chem. Soc.* **1976**, *98*, 4834.

Table 7. Experimental Metal and Sulfur K-edge XAS Energy Positions (eV)

	Metal K-edge			Sulfur K-edge	
	A[a]	B	C	pre-edge energy	near-edge Energy[b]
2	5990.04		5997.20	2469.75 2471.20	2472.53
1	5990.28		5996.95	2469.74 2471.31	2472.44
3[c]	5990.05		5996.68	2471.59	2472.29
4	5989.62 (sh) 5990.42 5992.37	5995.76	5998.01	2469.89 2471.14 2471.85	2472.72
5	5990.34 5992.42	5995.39	5997.70	2470.30 2471.52	2472.68
6	6540.32		6547.67	2470.40	2472.45
7	6540.34	6546.33	6549.29	2470.43 2471.92	2473.12
9	6540.32	6545.56	6547.67	2470.43	2472.40
8	6540.01	6545.12	6545.87	2470.33 2471.76	2472.38

[a] A, B, and C are defined in the text. [b] Lowest-energy edge transition. [c] Data are corrected for ~15% impurity of **1**.

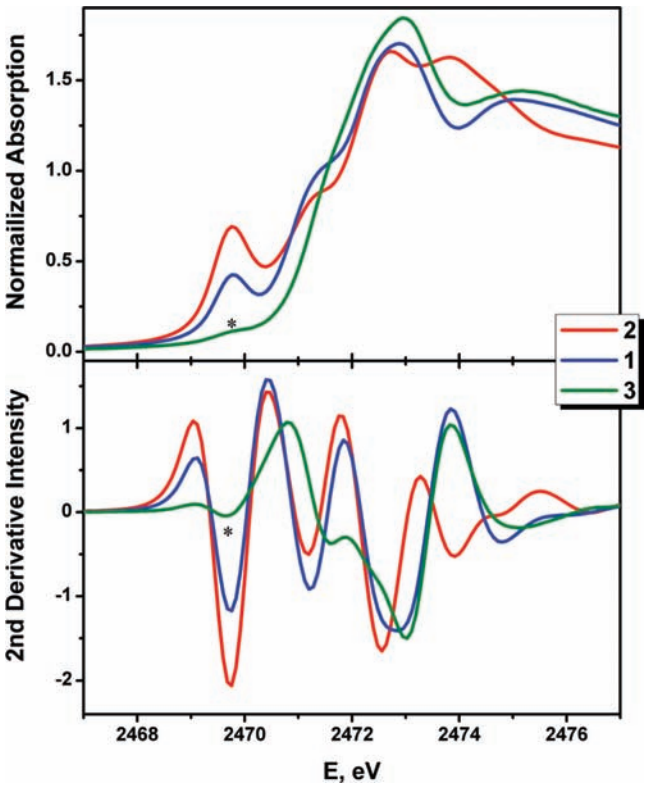

Figure 7. Comparison of the normalized S K-edge spectra of **1** (blue), **2** (red), and **3** (green), shown top and their second derivatives at the bottom (* in **3** denotes a 15% impurity of **1**).

a single, low-energy pre-edge peak at 2469.8, 2469.7, 2469.9 eV, respectively.[37,42] This peak is absent in the spectra of the trianions in **3** and **5** (a 15% impurity of **1** is present in the spectrum of **3**). A higher energy feature is observed at 2471.3 (**1**), 2471.2 (**2**), 2471.6 eV (**3**), respectively.[42,43] Previously, the spectrum of $[Cr(tbbdt)_3]^{1-}$

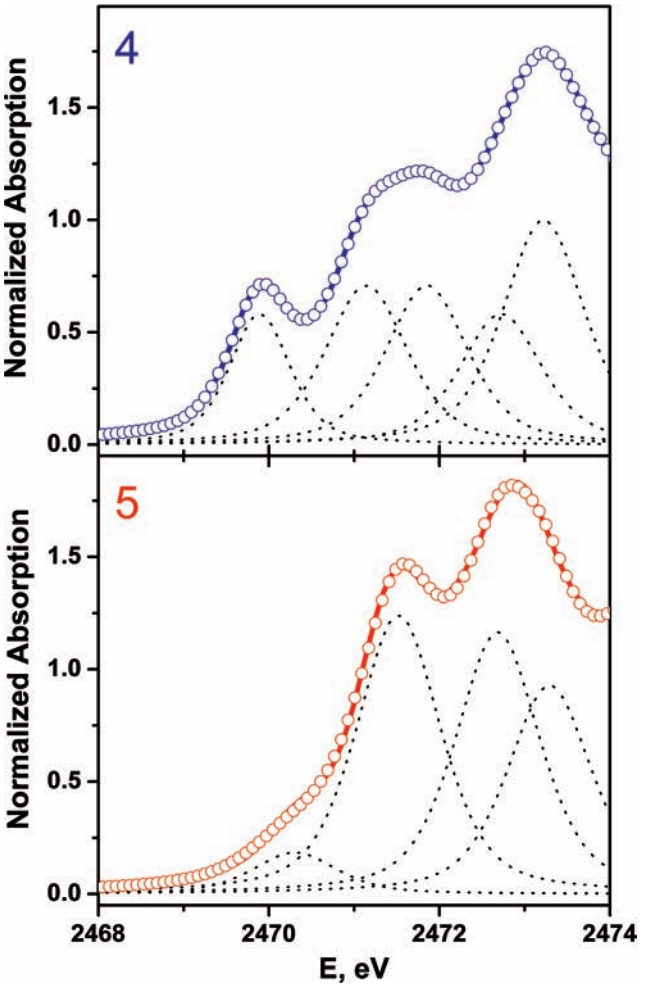

Figure 8. Pseudo-Voigt deconvolution of the S K-edge spectra of **4** and **5**. Circles represent the experimental data; dotted lines the pseudo-Voigt peaks; and the solid line is the sum of the fit.

has also been reported to display a lower energy feature at 2469.8 eV and a higher energy feature at 2471.2 eV, which resemble closely the present data for **2**.[4] The lower pre-edge feature at ~2469.8 eV has been assigned as a S 1s →3p transition reflecting ligand π radical character.[34,37,42−44] It is remarkable that the intensity of this peak increases on going from **2** to **1** by a factor of 2 which is, therefore, assigned a ligand-based oxidation. It indicates that the number of oxidative holes in the ligands of the trianion in **3** is zero but one in the dianion in **1** and two in the monoanion in **2**.

The spectrum of **4** displays the low-energy feature at 2469.9 eV indicating a ligand-based hole, $(mnt^{\bullet})^{1-}$, which is absent in the spectrum of **5**. Both spectra exhibit transitions at 2471.1, 2471.9, 2472.9 for **4** and 2470.3, 2471.5, 2472.7 eV for **5** (Figure 8), with the slight shift to higher energies in the latter because of partially oxidized sulfur atoms. The additional pre-edge feature, compared with **1**−**3**, stems from an excitation to low-lying C−N π^* of the mnt^{2-} ligand.[37] The area of the 1s → $mnt^{\bullet}$ transition at 0.492 units is derived from the pseudo-Voigt

(42) Kapre, R. R.; Bothe, E.; Weyhermüller, T.; DeBeer George, S.; Wieghardt, K. *Inorg. Chem.* **2007**, *46*, 5642.
(43) Tenderholt, A. L.; Szilagyi, R. K.; Holm, R. H.; Hodgson, K. O.; Hedman, B.; Solomon, E. I. *Inorg. Chem.* **2008**, *47*, 6382.
(44) (a) Solomon, E. I.; Hedman, B.; Hodgson, K. O.; Dey, A.; Szilagyi, R. K. *Coord. Chem. Rev.* **2005**, *249*, 97. (b) Szilagyi, R. K.; Lim, B. S.; Glaser, T.; Holm, R. H.; Hedman, B.; Hodgson, K. O.; Solomon, E. I. *J. Am. Chem. Soc.* **2003**, *125*, 9158.

deconvolution of the spectrum (Figure 8).[45] Notably, the area for equivalent excitation in **1** is significantly smaller at 0.248 units (Supporting Information, Figure S12); however, this intensity is consistent across the $[Cr(Cl_2\text{-}bdt)_3]^z$ series and appears to be inherent to the 1s → Cl_2-bdt$^\bullet$ transition.

The S K-edge spectra of the manganese complexes **6**, **7**, and **9** are all quite similar; they exhibit an intense pre-edge peak at ~2470.4 ± 0.1 eV indicating the absence of any valence hole in the ligands. It is remarkable that the $(dtc)^{1-}$ ligands in the monocationic species **9**, the $(Cl_2\text{-}bdt)^{2-}$ ligands in **6**, *and* the $(mnt)^{2-}$ ligands in **7** display this pre-edge peak at the same position and intensity. Since the peak energy is too high for a ligand radical transition and given the fact that dtc^{1-} is redox inert, we conclude that none of these species contains a ligand-based valence hole (no π radical character). Interestingly, the neutral complex **8** with a high-spin Mn(III) Jahn−Teller ion exhibits the pre-edge peak at 2470.3 eV (as do the other complexes) but the 2472.4 eV near-edge peak in **9** is split into two in **8** (2471.8 and 2472.4 eV) as shown in Figure 9. This might be a consequence of the presence of three shorter Mn−S bonds and three longer ones in **8** (Mn−S 2.385(1) Å and 2.582(1) Å).[13]

Furthermore, the intensity of the first pre-edge peak in **9** is approximately twice that of **8** (Figure 9), indicating that this peak is dominated by transitions to the e_g orbitals, which are singly occupied in **8** and empty in **9**. This is elaborated on using TD-DFT calculations. The above Mn and S K-edge spectra clearly demonstrate the absence of ligand-based oxidized π radical species. We are dealing with d^3 configurated Mn(IV) ions in **6**, **7**, and **9** whereas **8** contains a high-spin d^4 Jahn−Teller ion Mn (III). The ligands are either three closed-shell dithiolene dianions or three closed-shell dithiocarbamate(1−) monoanions.

Calculations. In this section, a picture of the electronic structures of complexes **1**−**5** and $[Cr(pdt)_3]^0$ is derived from broken symmetry (BS) DFT calculations by using the B3LYP functional for geometry optimizations, the MO descriptions, and spin distributions in these complexes. In our previous paper,[4] we have performed exactly the same type of calculations for the series $[Cr(tbbdt)_3]^z$ where z = 0, 1−, 2−, 3−. In general, the calculated geometries and metrical parameters of the anions in **1**, **2**, **3**, **4**, and **5** were found to be in very good agreement with experimental values where available (see Supporting Information). In particular, the geometry of all mono-, di-, and trianions is distorted octahedral (the calculated twist angles (Θ) exceeding 48° for complexes **1**, **2**, and **3** and >45° for **4** and **5**) in excellent agreement with experiment.

Similarly, the geometry of the manganese complexes **6** and **7** is close to regular octahedral, and the calculated twist angles and metrical parameters agree well with the experimental values (Supporting Information). The same is true for **8** and **9**. Interestingly, the Jahn−Teller distortion of the octahedral MnS_6 polyhedron of the Mn(III) complex **8** is well reproduced: three short calculated Mn−S distances at ~2.36 Å and three longer ones at ~2.52 Å (experiment: av. 2.395 and av. 2.509 Å).[13]

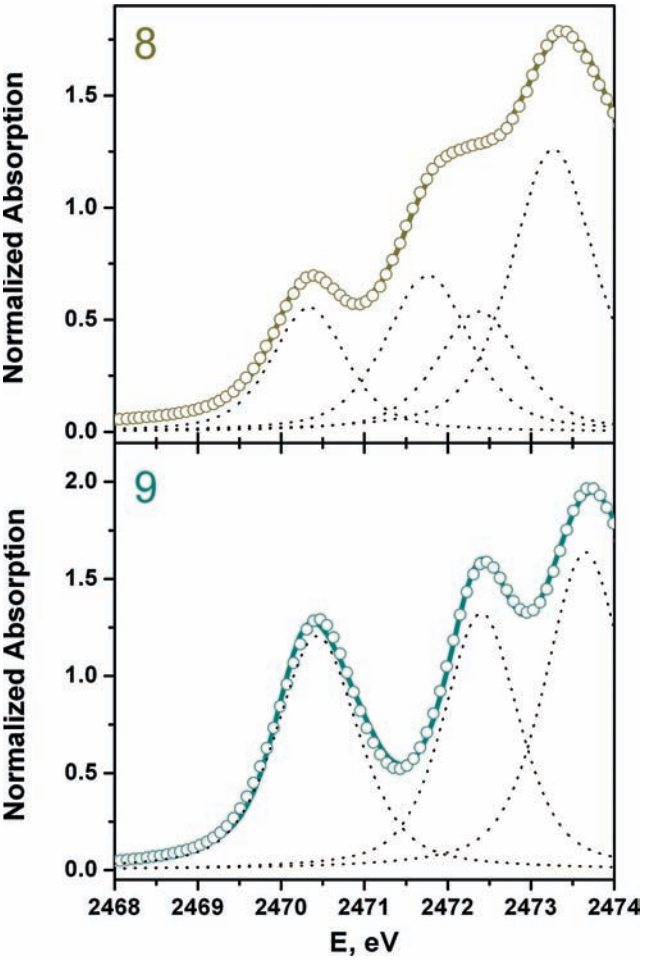

Figure 9. Pseudo-Voigt deconvolution of the resolved pre-edges (near-edges) of the neutral $[Mn(dtc)_3]$ in **8** (top) and its monocation $[Mn(dtc)_3]^+$ in **9** (bottom). Circles represent the experimental data; dotted lines the pseudo-Voigt peaks; and the solid line is the sum of the fit.

Quartet State Anions. The spin-unrestricted BP86 and B3LYP calculated electronic structures of the quartet state of the trianions in **3** (Figure 10), **5** (Supporting Information, Scheme S3) and the isoelectronic dianions in **6** (Figure 10), **7** (Supporting Information, Scheme S4), and in the monocation in **9** (Supporting Information, Scheme S6) revealed in all cases the presence of three singly occupied orbitals $(t_{2g})^3$ each of which possesses >86% metal d character. Thus, these compounds are typical octahedral chromium(III) or manganese(IV) species with a metal-centered d^3 electron configuration. Consequently, the calculated Mulliken spin densities show the presence of three unpaired electrons at the central metal ion. A small amount of spin polarization distributes spin density on the three ligands of the chromium complexes (in **3** there are 0.30 electrons distributed over six sulfur donor atoms; in **5** it is only 0.24 electrons) with a concomitant increase above 3 electrons on the Cr (III) centers. Similarly, 0.6 electrons are distributed over six sulfur atoms in **9**, 0.27 in **7**, and 0.48 in **6**, and indicates a greater amount of spin polarization by virtue of the larger Mn(IV) nuclear charge lowering energy difference between metal and ligand orbitals.

(45) George, G. N. *EXAFSPAK & EDG_FIT*, Stanford Synchrotron Radiation Laboratory, Stanford Linear Accelerator Center; Stanford University: Stanford, CA, **2000**.

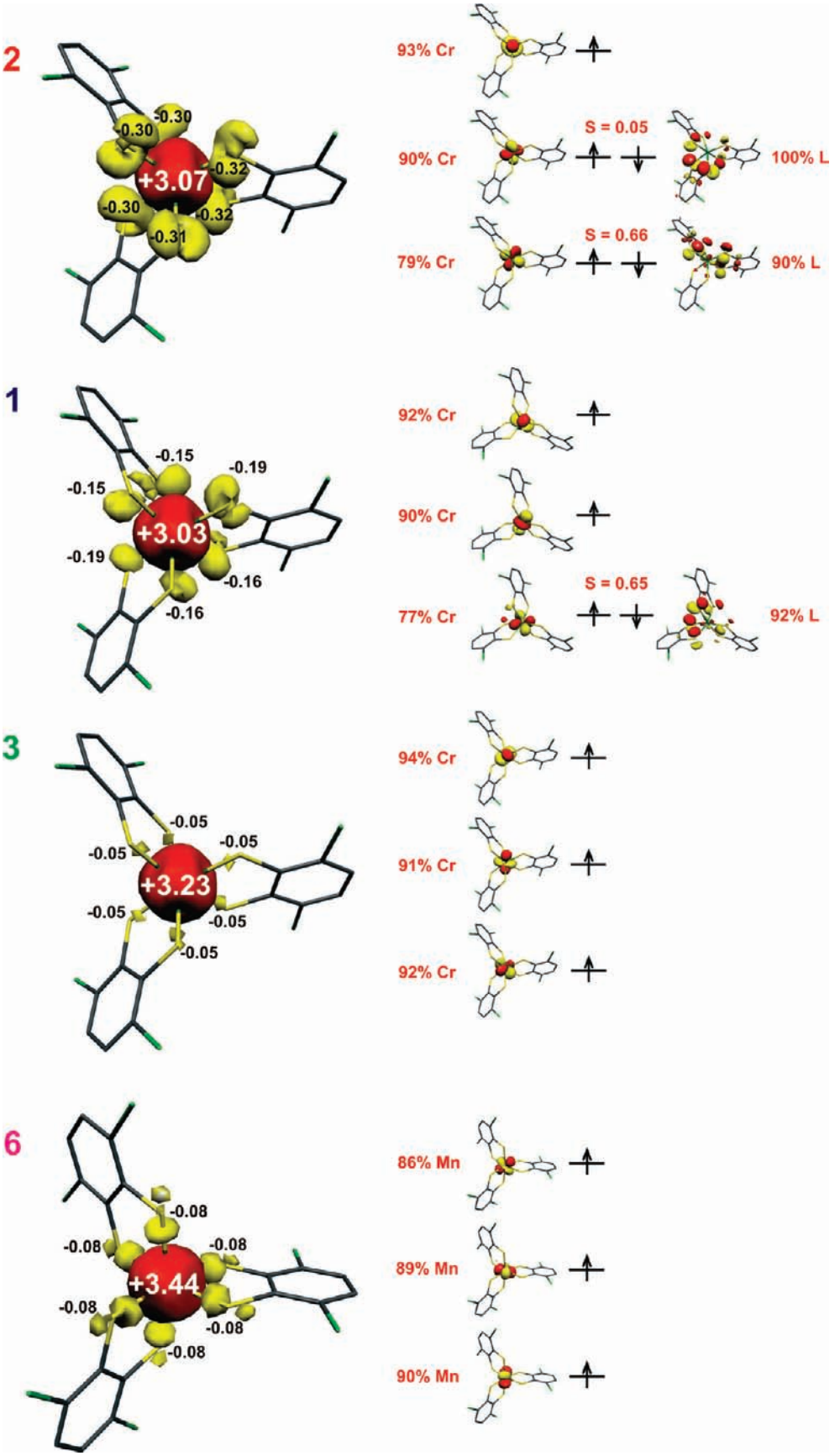

Figure 10. Spin density plots of the monoanion in **2**, the dianion in **1**, the trianion in **3**, and the dianion in **6**, as derived from BS DFT calculations for **2** and **1** and spin unrestricted Kohn−Sham calculations for the quartet state in **3** and **6**, together with values of the spin density of the Mulliken analyses. Qualitative MO diagrams of the corresponding orbital of magnetic pairs (**2** and **1**) and quasi-restricted orbitals (**3** and **6**) calculated at the B3LYP/TZVP level are shown right.

Triplet State Anions. The electronic structures of the following dianions, $[Cr(L)_3]^{2-}$, with an $S = 1$ ground state have been calculated using the BS(3,1) B3LYP method: $[Cr(Cl_2\text{-bdt}^{\bullet})(Cl_2\text{-bdt})_2]^{2-}$ (**1**) (Figure 10), and $[Cr(mnt^{\bullet})(mnt)_2]^{2-}$ (**4**) (Supporting Information, Scheme S2). The results for $[Cr(tbbdt^{\bullet})(tbbdt)_2]^{2-}$ have been reported.[4] Again three unpaired electrons identified (α-spin) in three metal-centered t_{2g}-type metal d-orbitals but one unpaired electron (β-spin) is distributed over six sulfur atoms. This qualitative MO scheme holds for the three complexes mentioned above. The ligand spin ($S_{rad} = {}^1/_2$) couples antiferromagnetically ($S = 0.65$) with the intrinsic $S_{Cr} = {}^3/_2$ spin of the central chromium ion affording the observed $S_t = 1$ ground state. A coupling constant ($H_{ex} = -2J_{GS}\mathbf{S}_1\cdot\mathbf{S}_2$), J of -175 cm^{-1} has been calculated for $[Cr^{III}(tbbdt^{\bullet})(tbbdt)_2]^{2-}$.[4] Thus, one-electron oxidation of **3** to **1** (or **5** to **4**) is a ligand-centered process.

Doublet State Anions. The electronic structures of the monoanions in **2** (Figure 10) and the hypothetical $[Cr(mnt^{\bullet})_2(mnt)]^{1-}$ (Supporting Information, Scheme S1) with an $S_t = {}^1/_2$ ground state have been calculated as described above by using the BS(3,2) method. Again similar calculations for $[Cr(tbbdt^{\bullet})_2(tbbdt)]^{1-}$ have been reported and shown to closely corroborate the experimental data.[4] A typical Cr(III) ion with ~3 unpaired electrons in predominantly metal d-orbitals (t_{2g}) have been identified (α-spin in Figure 10) and ~1.8 unpaired β-electrons are distributed over the six S atoms indicating the presence of two ligand-centered valence holes in all three species. The ligand spins are antiferromagnetically coupled (S = 0.66 and S = 0.06) to the Cr(III) ion yielding the observed $S_t = {}^1/_2$ ground state. It is noted that $[Cr(mnt^{\bullet})_2(mnt)]^{1-}$ has not been isolated; however, the X-band EPR spectrum is nearly identical to that of **2** and other recorded $[Cr(L)_3]^{1-}$.[1,2,4] These calculations dismiss the presence of a Cr(V) ion and three closed-shell dithiolate(2-) ligands and instead show oxidation of **1** and **4** as ligand-centered.

Singlet State Neutral Species. The BS(3,3) B3LYP DFT calculations of $[Cr^{III}(tbbdt^{\bullet})_3]^0$ have been described in ref 4. A central Cr(III) ion is S,S'-coordinated to three antiferromagnetically coupled π radical ligand monoanions, $(tbbdt^{\bullet})^{1-}$, yielding the observed $S = 0$ ground state. Interestingly, the calculated geometry of the CrS_6 polyhedron is nearly octahedral (av. $\Theta = 47.9°$). Attempts to isolate this compound have not proven successful, so we rely solely on DFT calculations to predict the electronic structure and spectroscopic properties. Of the two known [tris(dithiolene)chromium] neutral complexes, we have calculated a similar complex $[Cr(pdt)_3]^0$ containing a type B dithiolene ligand (Scheme 1).[2] The geometry optimization has been carried out by using the atom coordinates of the crystallographically characterized, trigonal prismatic $[V(pdt)_3]^0$,[46] where we replaced the vanadium by a chromium ion and adjusted the spin state from $S_V = {}^1/_2$ to $S_{Cr} = 0$. A spin unrestricted $S = 0$ calculation for $[Cr(pdt)_3]^0$ resulted in a trigonal prismatic structure ($\Theta = 4.3°$) as shown in Figure 11b. Using these as starting coordinates but implementing the BS(3,3) method for a reoptimization, results in the structure twisting to octahedral ($\Theta = 49.7°$, Figure 11a). When we used these octahedral coordinates but removed the broken symmetry flag, the structure reverts to the trigonal prismatic geometry. Most crucially, the total energy difference between the two different minima is 18.9 kcal mol^{-1} *in favor of the octahedral structure*. The electronic structure is then clearly established as shown in Figure 11a.

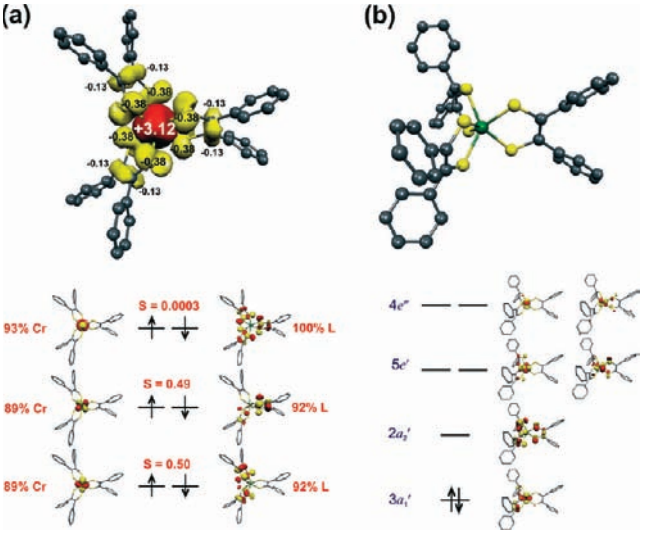

Figure 11. Calculated electronic structures of the neutral complex $[Cr(pdt)_3]^0$ ($S = 0$). (a) The octahedral solution from BS(3,3) B3LYP showing the Mulliken spin density plot and qualitative MO diagram of the corresponding orbitals of magnetic pairs (S represents the orbital overlap integral). (b) The trigonal prismatic solution from a spin-unrestricted Kohn–Sham calculation showing the Mulliken spin density plot with no unpaired electrons and qualitative MO scheme of canonical orbitals.

Three singly occupied (α-spin) metal d-orbitals (t_{2g}) (~89% Cr) are identified which are antiferromagnetically coupled to three ligand π radical ligands, $(pdt^{\bullet})^{1-}$, affording the observed singlet ground state. It is interesting to note that the calculated av. C–S and C–C distances at 1.724 Å and 1.410 Å, respectively, in $[Cr^{III}(pdt^{\bullet})_3]$ are very close to those reported for $[Pt^{II}(^{tBu}pdt^{\bullet})_2]$ at av. 1.71 and 1.39 Å, respectively.[47] The average Cr–S distance at 2.393 Å is slightly overestimated compared with values found experimentally for **1**, **4**, **5** and $[Cr(tbbdt^{\bullet})_2(tbbdt)]^{1-}$ at 2.332, 2.344, 2.394, and 2.299 Å, respectively. This overestimation is typical for the B3LYP functional. The spin density plot shown in Figure 11a clearly shows three unpaired electrons at the Cr center (α-spins) and one unpaired electron per ligand π radical monoanion (β-spin). Interestingly, 76% of the ligand spin density resides on the sulfur donor atoms, and only 24% resides at the two "olefinic" carbon atoms per ligand. This is the typical spin density distribution for a sulfur-centered radical. Conversely, the calculated MO scheme for the trigonal prismatic solution exhibits the a_1', e', e'' ligand field splitting of D_{3h} symmetry with the d_{z^2} ($3a_1'$) doubly occupied. The electronic structure is formulated as $[Cr^{IV}(pdt^{\bullet})_2(pdt)]^0$ where the two ligand "radicals"

(46) Eisenberg, R.; Gray, H. B. *Inorg. Chem.* **1967**, *6*, 1844.

(47) Pap, J. S.; Benedito, F. L.; Bothe, E.; Bill, E.; DeBeer George, S.; Weyhermüller, T.; Wieghardt, K. *Inorg. Chem.* **2007**, *46*, 4187.

Table 8. Comparison of Calculated and Experimentally Determined Metal and Sulfur K-pre-Edge Energies (eV) of the Complexes

	metal K-edge		sulfur K-edge	
	calcd[a]	exptl	calcd[b]	exptl
$[Cr(tbbdt)_3]^{1-}$	5989.64 (sh)		2469.51	2469.79
	5990.37		2470.70	
			2471.29	2471.19
2	5989.38		2469.40	2469.75
	5990.46	5990.04	2470.67	
			2471.34	2471.20
1	5988.62		2469.37	2469.74
	5990.36	5990.28	2471.18	2471.31
3	5989.99	5990.05	2471.35	2471.59
4	5989.07	5989.62 (sh)	2469.64	2469.89
	5990.34	5990.42	2471.33	2471.14
		5992.37		2471.85
5	5990.02	5990.34	2470.94	2470.30
		5992.42		2471.52
6	6540.38	6540.32	2470.40	2470.43
			2471.78	2472.41
7	6540.32	6540.34	2470.65	2470.41
			2471.37	2471.92
8	6540.16 (sh)	6540.32	2470.22	2470.33
	6541.11		2471.49	2471.76
9	6540.35	6540.01	2470.56	2470.43
			2471.79	2472.40

[a] Energy shift of +154.9 eV (Cr) and +169.4 eV (Mn). [b] Energy shift of +77.0 eV.

manifest as the empty ligand-centered $2a_2'$ MO;[48] thus there are no unpaired electrons in the molecule.

Time-Dependent Density-Functional Calculations. Cr and Mn K-pre-edge XAS. Very recently, a simple time-dependent DFT (TD-DFT) approach was developed for the calculation of pre-edge XAS spectra[29,30] and successfully utilized in assigning S, Cl, Mn, and Fe K-edge XAS spectra.[33−35] We have used this method in calculating the metal K-edge spectra with the results summarized in Table 8. The pre-edge region of metal (Cr and Mn) K-edge spectra reveal peaks from weak quadrupole-allowed 1s → 3d transitions, which primarily gain intensity through mixing of 4p character into these orbitals giving the transitions significant electric dipole character.

The calculated Cr K-pre-edge spectra for **1**, **2**, and **3** are shown in Figure 14 and afford an excellent fit of the experimental data. The calculated absolute energies were found to be lower in energy by 154.9 eV than the experimental values. Most interestingly, the calculations replicate, with a slight underestimation, the low-energy shoulder in the pre-edge region of the monoanion in **2** (Figure 12) and the dianions of **1** (Figure 12) and **4** (Supporting Information, Figure S21), though this is only experimentally apparent in the latter. The resolution is insufficient to expose these spectroscopic details and result in pre-edge regions quite sensitive to the pre-edge subtraction and normalization. For **2**, there are two transitions to these two orbitals at 5989.38 eV, which lie adjacent to a peak at 5990.36 eV that broaden the

(48) For trigonal prismatic $[Cr^{IV}(pdt^{\bullet})_2(pdt)]^0$, there are no unpaired electrons in the molecule as the two ligand "radicals" are the empty $2a_2'$ MO. As such the ligand system is more accurately described as $[(dithiolene)_3]^{4-}$ with two "holes" distributed over the three ligands. However, we continue to use the "$L^{\bullet}$" notation for simplicity and consistency with octahedral tris(dithiolene) complexes and square planar bis(dithiolene) analogues.

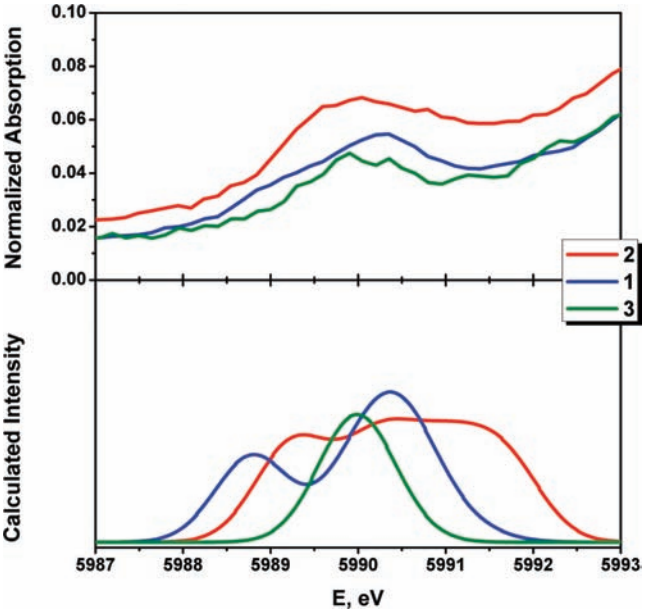

Figure 12. Experimental (top) and calculated (bottom) Cr K-pre-edge XAS spectra of the monoanion in **2**, the dianion in **1**, and the trianion in **3** obtained from BP86 TD-DFT calculations. Calculated intensity in arbitrary units.

pre-edge region of the spectrum, and result from excitation to the two lowest unoccupied MOs (LUMOs) of the complex: the α-spin orbitals of the ligand π radicals. The transition assignment for **2** is shown in Figure 13.

A stick plot in Figure 13 shows the dipole and quadrupole contributions to the calculated transition intensity and the composition of the acceptor MOs are listed in Table 9. Despite the low Cr 3d content of these MOs, they are relatively intense because of a small but crucial contribution from the Cr 4p orbitals (0.8 and 1.1%). The second peak is the 1s excitation to the three $t_{2g}(\beta)$ MOs, while the last two peaks are 1s → $e_g(\alpha)$ and 1s → $e_g(\beta)$ transitions, respectively. It can been seen that the dipole contribution to the intensity of the 1s → $t_{2g}(\beta)$ transitions results from a small 4p content, which is negligible in the e_g MOs. The first peak in the spectrum of **1** is the 1s → $L^{\bullet}(\alpha)$ transition, while the second peak comprises the 1s → $t_{2g}(\beta)$ and 1s → $e_g(\alpha)$ transitions and thus precludes comparison of calculated and experimental oscillator strengths. Again, their relative intensities are proportional to the 4p character of the acceptor orbital (Table 9).

The calculated Mn K-pre-edge regions for complexes **6**−**9** are displayed in Figure 14 and here again the TD-DFT method reasonably replicates the spectral features after shifting the calculated energies by +169.4 eV. Experimental values for the four Mn complex are nearly identical, with a difference of only 0.3 eV between $[Mn^{III}(dtc)_3]^0$ and $[Mn^{IV}(dtc)_3]^+$, where there is a formal change in the oxidation state. While the rising edge for the former clearly shows a more reduced Mn center, calculations produce a shoulder at lower energy (6539.82 eV) assigned as the 1s to the unoccupied e_g orbital (LUMO) in this high-spin Mn(III) d^4 system. Its weak intensity stems from the absence of Mn 4p character. The equivalent transitions for **9** are calculated at 6540.44 eV, which represents a difference of 0.62 eV associated with a formal

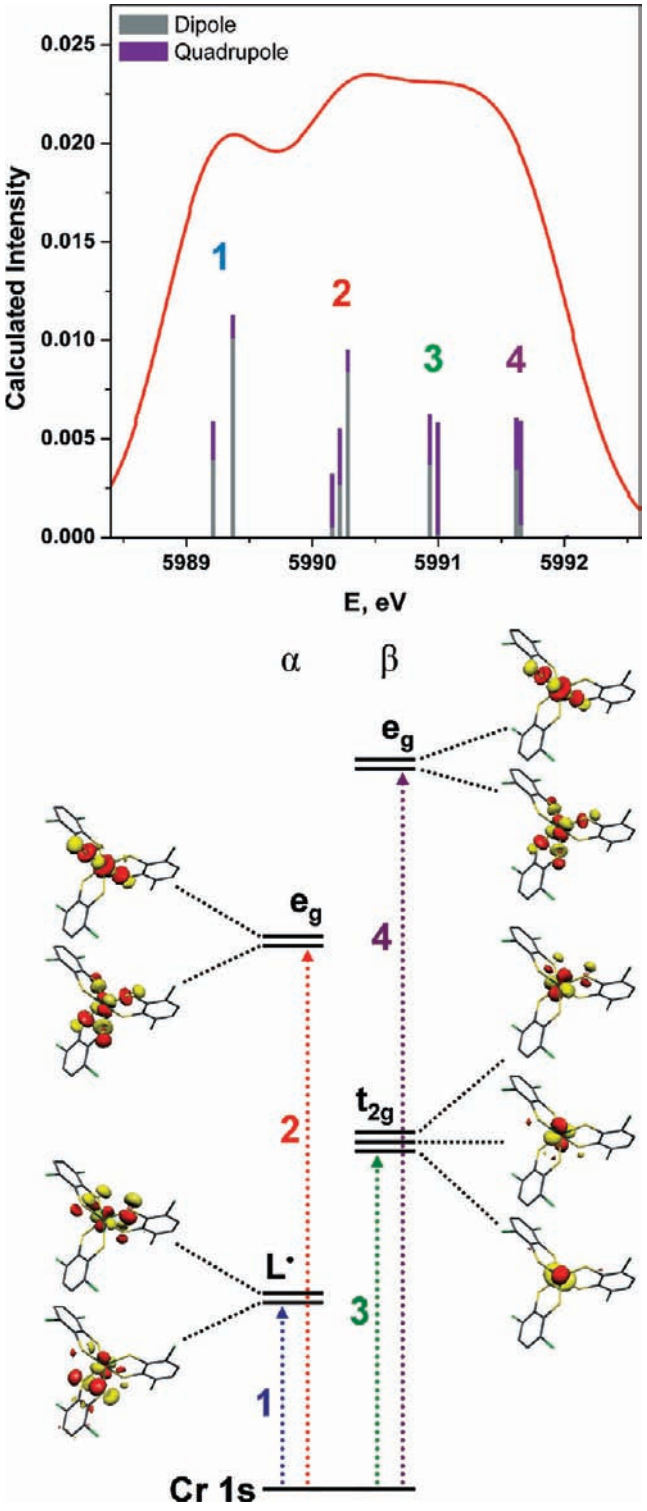

Figure 13. Top: Simulated Cr K-pre-edge spectrum of **2** (red) and stick plot showing the dipole (gray) and quadrupole (purple) contributions to the pre-edge transitions. The total calculated intensity is the sum of these components in arbitrary units. Bottom: A qualitative MO scheme presents the lowest unoccupied orbitals derived from a BP86 DFT calculation of **2** and the four transitions that comprise the calculated pre-edge. The MO compositions are displayed in Table 9.

change in the Mn oxidation state. For both complexes, the $1s \rightarrow t_{2g}(\beta)$ occur at the same energy (~6540.2 eV). As noted before, e_g orbitals in octahedral symmetry have no metal 4p character and the weak intensity results from the

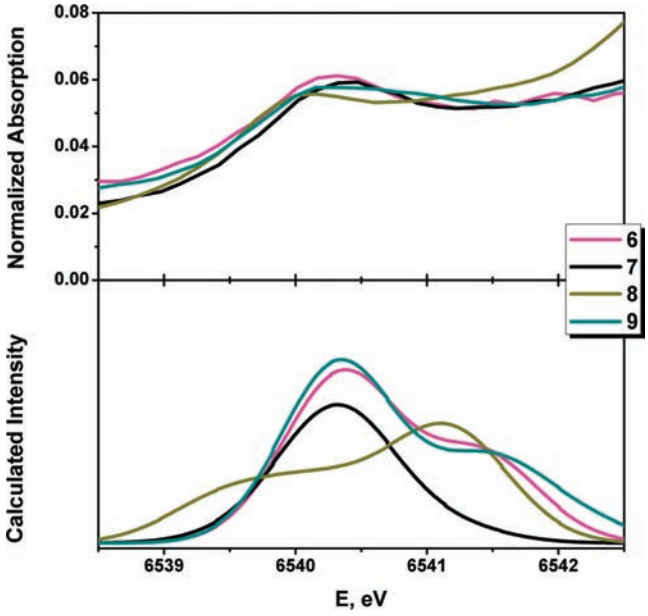

Figure 14. Experimental (top) and calculated (bottom) Mn K-pre-edge spectra for **6**−**9** obtained from BP86 TD-DFT calculations. Calculated intensity in arbitrary units.

Table 9. Cr 3d and 4p Contributions to the Lowest Unoccupied Orbitals of **1**−**3** Derived from BP86 DFT Calculations

	2		**1**		**3**	
	3d	4p	3d	4p	3d	4p
L•(α)	31.2	0.8				
	31.6	1.1	35.5	1.4		
$t_{2g}(\beta)$	76.4	0.0	70.9	0.0	50.4	0.0
	72.7	0.4	71.3	0.6	41.3	0.1
	68.9	0.5	66.0	0.3	40.2	0.1
$e_g(\alpha)$	52.0	0.1	53.0	0.1	56.7	0.1
	52.4	0.0	54.2	0.0	56.9	0.1

absence of an electronic dipole contribution. In contrast, the $t_{2g}(\beta)$ set have 0.2−0.3% 4p character which amplifies the intensity of transitions to these orbitals.

Sulfur K-pre-Edge XAS. The experimental and calculated S K-edge XAS spectra for the series **2**, **1**, and **3** are shown in Figure 15 with the peak energies listed in Table 8. For the monoanion in **2** and the dianion in **1** two pre-edge transitions are at calculated energies (shifted by +77.0 eV) of 2469.40, 2471.34 eV and 2469.37, 2471.18 eV, respectively, with a shoulder evident at 2470.67 eV in **2**. It is significant that the calculated S K-edge spectrum of **3** lacks the above first low-energy transition, and only one pre-edge transition at 2471.01 eV is calculated in excellent agreement with experiment (2471.59 eV). The relative intensity of the first two transitions in **2** is calculated as 1.00:1.05 and is an underestimation of the experimental intensity ratio of 1.00:1.50. However, while the linewidth (fwhm) for the $1s \rightarrow L^{\bullet}$ peak is indicative of a one-electron transition (0.88 eV), the second peak is considerably larger at 1.34 eV, and confirms more than one transition contributes to this peak. This second peak is a composition of transitions to the $t_{2g}(\beta)$ and $e_g(\alpha)$ orbitals (Figure 13). Similarly for **1**, the first peak is the $1s \rightarrow L^{\bullet}$ transition while the second is a broad envelope of $1s \rightarrow t_{2g}(\beta)$ and $1s \rightarrow e_g(\alpha)$ transitions.

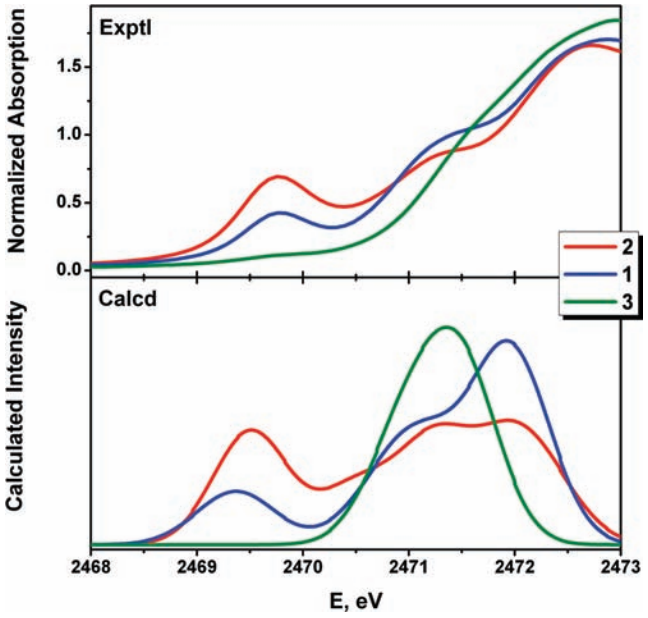

Figure 15. Experimental (top) and calculated (bottom) S K-edge XAS spectra of the monoanion in **2**, the dianion in **1**, and the trianion in **3** obtained from BP86 TD-DFT calculations. Calculated intensity in arbitrary units.

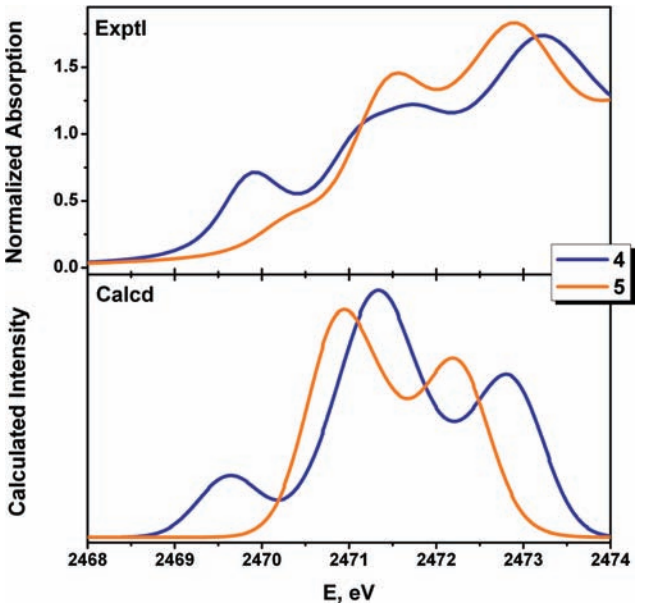

Figure 16. Experimental (top) and calculated (bottom) S K-edge XAS spectra of **4** and **5** obtained from BP86 TD-DFT calculations. Calculated intensity in arbitrary units.

Moreover, the intensity of the radical peak is exactly half that for **2**, and clearly demonstrates the presence of one oxidized ligand in **1**, with two in **2**. The dianion in **4** exhibits the two transitions described for **1** with an additional peak from excitation to the low-lying C−N π^* orbital (Figure 16).[37] The near-edge features are dominated by transitions to C−S π^* MOs that reside just above the e_g orbitals in these complexes (Figure 15).

An experimental oscillator strength of 5.04×10^{-4} for the $1s \rightarrow L^{\bullet}$ transition is extracted from the pseudo-Voigt deconvolution of **4** (Figure 8) and compares nicely with the calculated value of 3.82×10^{-4} derived from TD-DFT calculations.[49] The estimated S 3p character of 42.9% agrees well with the 48.9% character in the $(mnt^{\bullet})^{1-}$ MO determined from the BP86 ground state calculation. However, for **1** and **2**, there is a marked difference between experiment and calculated values, such that the calculated S 3p content is twice that observed experimentally. Despite the observed air and temperature instability of **1**−**3** these samples show (by proton NMR) no signs of free-ligand or any other sulfur impurity that could produce this low pre-edge intensity, such that at this stage we are unable to account for this anomaly. However, the relative intensity of this transition to the ligand radical is consistent across the series.

Similarly, the spectra of the isoelectronic Mn(IV) complexes **6**, **7**, and **9** (Figure 17) have been calculated with one transition at ~2470.5 ± 0.2 eV again in excellent agreement with experiment (2470.4 eV). The calculations reveal the intense pre-edge peak is due to a combination of $1s \rightarrow t_{2g}(\beta)$ and $1s \rightarrow e_g(\alpha)$ transitions, and ~1 eV lower in energy than the same peak in the Cr complexes. This is due to the larger effective nuclear charge of Mn(IV) ion

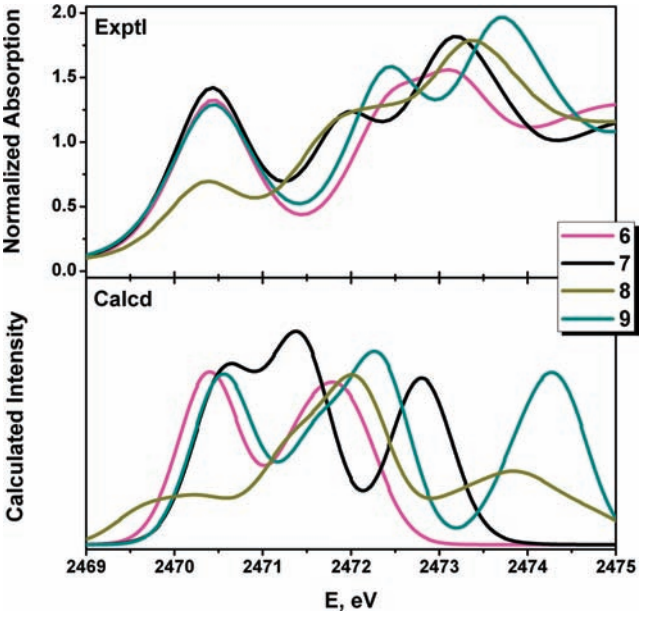

Figure 17. Experimental (top) and calculated (bottom) S K-edge XAS spectra of **6**−**9** obtained from BP86 TD-DFT calculations. Calculated intensity in arbitrary units.

compared with Cr(III). This peak is still 1 eV higher in energy than the radical anion pre-edge peak in **1**, **2**, and **4**, and confirms the absence of an oxidized ligand in **6** and **7**. This is further confirmed by the existence of same peak, both in energy and intensity, in **9** with redox innocent $(dtc)^{1-}$ ligands. The experimental spectrum of the Mn(III) complex **8** shows two broad transitions at 2470.33 and 2471.76 eV. The calculated spectrum produces a very broad peak at 2470.22 eV which is a consequence of the Jahn−Teller distortions leading to two different Mn−S distances with differing Mn−S covalency. However, the calculated intensity ratio for this peak in **8** compared to **9** is 1.00:2.05, quite similar to the 1.00:2.41 experimental ratio.

(49) Calibrated to $[Au(bdt)_2]^0$, where the transition area for a excitation to a π-acceptor orbital is 0.708 units corresponds to 60% S 3p character; Ray, K.; DeBeer George, S.; Solomon, E. I.; Wieghardt, K.; Neese, F. *Chem, Eur. J.* **2007**, *13*, 2783.

Discussion

In the following, we discuss pertinent molecular and electronic aspects of each member of the electron transfer series $[Cr(L)_3]^z$ (z = 0, 1−, 2−, 3−) where L represents a dithiolene ligand of type A or type B (Scheme 1) and compare the results with those reported recently for the analogous series of molybdenum and tungsten complexes.[42,43] It is unequivocally established that the trianionic chromium species $[Cr(L)_3]^{3-}$ where L represents an *S*,*S*′-coordinated bidentate dithiolene ligand of type A or B possess a distorted octahedral CrS_6 polyhedron with an average twist angle $\Theta \approx 50°$. These trianions possess an $S = {}^3/_2$ ground state which is in accord with a central Cr(III) ion and three unpaired electrons residing in three metal-centered d-orbitals, $(t_{2g})^3$, which renders the three dithiolene ligands closed-shell dianions. Thus, complexes **3** and **5** are best described as classic Werner-type complexes: $[Cr^{III}(Cl_2\text{-bdt})_3]^{3-}$ and $[Cr^{III}(mnt)_3]^{3-}$. This description is in accord with their X-band EPR spectra and electronic spectra. Cr and S K-edge XAS provides strong evidence that the dithiolato (2−) ligands do not possess an oxidative valence hole (no π radical character). These results are in full agreement with the corresponding octahedral trianions $[Cr^{III}(catecholate)_3]^{3-}$ ($S = {}^3/_2$) containing three closed-shell catecholate(2−) dianions and a central Cr(III) ion.[4,41] Spin-unrestricted DFT calculations ($S = {}^3/_2$) are also in excellent agreement with these assignments, since the calculated spin density distribution clearly shows three unpaired electrons at the metal ion and virtually no spin density on the dithiolene ligands (∼0.05 per sulfur atom). Similarly, the isoelectronic manganese dianions in **6** and **7**, also possess an $S = {}^3/_2$ ground state as elucidated from X-band EPR spectroscopy and magnetic susceptibility measurements. The central manganese ion is Mn(IV) with a $(t_{2g})^3$ configuration. Both complexes are nearly octahedral. The dithiocarbamate monocation $[Mn^{IV}(dtc)_3]^+$ is also distorted octahedral and possess an $S = {}^3/_2$ ground state. One-electron reduction of **9** produces the neutral species $[Mn^{III}(dtc)_3]$ (**8**) with an S = 2 ground state. The Mn K-edges of **8** and **9** clearly show that the electron transfer is metal-centered, and S K-edge XAS spectra demonstrate that in both cases three closed-shell $(dtc)^{1-}$ ligands are present. The analogous S K-edge XAS spectra of **6** and **7** clearly show that only closed-shell dithiolene dianions are present. Again the DFT calculations corroborate these descriptions of the electronic structures of complexes **6**−**9**. These octahedral Werner-type coordination compounds of Cr(III) and Mn(IV) represent benchmark cases for tris(dithiolene)metal complexes containing three closed-shell dithiolates and a central paramagnetic d^3 metal ion; they serve to calibrate our spectroscopies and DFT calculations. In the following we will closely monitor changes of the electronic structure upon stepwise one-electron oxidations of the trianions $[Cr(L)_3]^{3-}$ via the di-, to the monoanions and, finally, to the neutral species $[Cr(L)_3]^0$.

The structurally characterized dianion $[Cr(Cl_2\text{-bdt})_3]^{2-}$ in **1** possesses distorted octahedral CrS_6-polyhedron and an $S = 1$ ground state (two unpaired electrons). The same is true for $[Cr(mnt)_3]^{2-}$.[7] Considering the electronic structure of the trianions as described above the question arises whether the one-electron oxidation is metal-centered yielding a Cr(IV) ion (d^2, two unpaired electrons) and three closed-shell dianionic ligands or is ligand-centered affording a central Cr(III) ion (d^3) with a sulfur valence hole (distributed over all six sulfur donors). Cr and S K-edge XAS spectroscopy unequivocally shows that the latter is the case: $[Cr^{III}(Cl_2\text{-bdt}^{\bullet})(Cl_2\text{-bdt})_2]^{2-}$. This spectroscopic result is corroborated by a BS(3,1) DFT calculation where three singly occupied metal d-orbital have been identified (α-spin) which couple antiferromagnetically to one singly occupied ligand π-orbital (β-spin). The unpaired electron is distributed over all six sulfur donors (delocalized). It is interesting to compare this result with three "isoelectronic", dianionic [tris(dithiolene)molybdenum]$^{2-}$ species, namely, $[Mo^{IV}(mdt)_3]^{2-}$,[50] $[Mo^{IV}(qdt)_3]^{2-}$,[51] and $[Mo^{IV}(mnt)_3]^{2-}$,[52] where $(qdt)^{2-}$ represents the closed-shell dianion *o*-quinoxalinedithiolate-(2−), a type A dithiolene. All have an S = 0 ground state with the latter possessing a trigonally twisted MoS_6 polyhedron (Θ = 28.2°), while the others are trigonal prismatic (Θ = 2.6° and 4.5°, respectively). S K-edge spectra of these species indicate the absence of a ligand-centered valence hole (no π radical monoanion is present).[43,53] Thus, their electronic structure is correctly described as Mo(IV) (d^2, S = 0) species with three *S*,*S*′-coordinated dithiolate (2−) ligands.

The structurally characterized monoanion $[Cr(tbbdt)_3]^{1-}$ possesses a distorted octahedral CrS_6 polyhedron and an $S = {}^1/_2$ ground state.[4] The similarity of its electronic spectrum with that of **2** suggests a similar molecular and electronic structure for the latter. The similar Cr K-pre-edge peak energy (Cr 1s → 3d) of **1**, **2**, and **3** clearly indicate the presence of a central Cr(III) ion in all three cases. The S K-edge spectrum of **2** clearly exhibits a low-energy pre-edge peak with twice the intensity as that observed in **1**. Thus, a Cr (III) ion is antiferromagnetically coupled to two ligand π radical monoanions: $[Cr^{III}(Cl_2\text{-bdt}^{\bullet})_2(Cl_2\text{-bdt})]^{1-}$. Comparison with the corresponding monoanions of molybdenum $S = {}^1/_2$, namely, $[Mo(mdt)_3]^{1-}$,[54] $[Mo(tbbdt)_3]^{1-}$,[42] and $[Mo(qdt)_3]^{1-}$,[55] is revealing in that the S K-edge XAS spectrum of $[Mo(mdt)_3]^{1-}$ reveals a low-energy pre-edge peak at ∼2470.1 eV characteristic of the presence of a ligand-centered valence hole.[43] An electronic structure of $[Mo^{IV}(mdt^{\bullet})(mdt)_2]^{1-}$ with a ligand valence hole yielding a half-filled ligand π orbital is observed. Note that $(mdt)^{2-}$ is a type B ligand. In stark contrast, for $[Mo(tbbdt)_3]^{1-}$ and $[Mo(qdt)_3]^{1-}$ we do not observe a corresponding low-energy pre-edge peak in the S K-edge spectrum ($(tbbdt)^{2-}$ and $(qdt)^{2-}$ are type A).[42,53] Thus, this complex possesses a central Mo^V (d^1) ion with three closed-shell dithiolates(2−): $[Mo^V(tbbdt)_3]^{1-}$ ($S = {}^1/_2$). Consequently, in the Mo K-edge XAS spectra of $[Mo^{IV}(qdt)_3]^{2-}$ and $[Mo^V(qdt)_3]^{1-}$ (both of which are trigonal prismatic) the rising edge energy increases by ∼0.9 eV[53] which is typical for a change of the metal oxidation number by 1 unit.

Again in contrast, the Mo L_3-edge XAS data for $[Mo^{IV}(mdt)_3]^{2-}$ and $[Mo^{IV}(mdt)_3]^{1-}$ have been reported to be nearly identical indicating the presence of a Mo(IV) ion in

(50) Formitchev, D.; Lim, B. S.; Holm, R. H. *Inorg. Chem.* **2001**, *40*, 645.
(51) Boyde, S.; Garner, C. D.; Enemark, J. H.; Bruck, M. A.; Kristofzski, J. G. *J. Chem. Soc., Dalton Trans.* **1987**, 2267.
(52) Brown, G. F.; Stiefel, E. I. *Inorg. Chem.* **1973**, *12*, 2140.
(53) Sproules, S.; DeBeer George, S.; Wieghardt, K., unpublished results.
(54) Lim, B. S.; Donahue, J.; Holm, R. H. *Inorg. Chem.* **2000**, *39*, 263.
(55) Boyde, S.; Garner, C. D.; Enemark, J. H.; Bruck, M. A. *J. Chem. Soc., Dalton Trans.* **1987**, 297.

both species which is in accord with an electronic structure $[Mo^{IV}(mdt^{\bullet})(mdt)_2]^{1-}$.[43] The L_3-edge energy is dominated by ligand-field splitting rather than effective nuclear charge, so the result is not so surprising since both anions are trigonal prismatic ($\Theta = 2.6°$ and 1.6°, respectively).[50,54] Nevertheless, *the electronic structure of the monoanionic [tris(dithiolene)-molybdenum]$^{1-}$ complexes is dependent on the nature of the dithiolene ligand (type A or B).*[43] If the ligand is of type A the electronic structure is $[Mo^{V}(L)_3]^{1-}$ with a metal-centered half-filled d-orbital $(d_{z^2})^1$ but if it is of type B the electronic structure is $[Mo^{IV}(L^{\bullet})(L)_2]^{1-}$ with a filled $(d_{z^2})^2$ orbital and a valence hole in the ligands (π radical character). It is notable that the structure of $[Mo^{V}(tbbdt)_3]^{1-}$ is intermediate octahedral-trigonal prismatic ($\Theta = 31.7°$)[42] but that of $[Mo^{IV}(mdt^{\bullet})(mdt)_2]^{1-}$ is trigonal prismatic ($\Theta = 1.6°$).[54] For monoanionic [tris(dithiolene)chromium]$^{1-}$ complexes the electronic structure is $[Cr^{III}(L^{\bullet})_2(L)]^{1-}$ with a central Cr(III) d^3 and two ligand-centered valence holes (π radicals) irrespective of the nature of the ligand, type A or B. The similarity of the electronic absorption and EPR spectra for $[Cr^{III}(Cl_2\text{-}bdt^{\bullet})_2(Cl_2\text{-}bdt)]^{1-}$ (type A dithiolene), and $[Cr^{III}(mnt^{\bullet})_2(mnt)]^{1-}$, $[Cr^{III}(pdt^{\bullet})_2(pdt)]^{1-}$, and $[Cr^{III}(tfd^{\bullet})_2(tfd)]^{1-}$ (type B dithiolenes),[1,2] shows all have the same electronic and molecular structure.

The discussion of the electronic structure of the neutral tris(dithiolene)chromium complexes is hampered by the fact that no crystal structure of any of these species has been reported to date and importantly, the Cr and S K-edge XAS data are also not available. Early workers have suggested a trigonal prismatic CrS_6 polyhedron for $[Cr(pdt)_3]$ which was solely based on the observed "isomorphism" of this species with those of $[V(pdt)_3]^0$,[46] $[V(pdt)_3]^{1-}$,[56] and $[Mo(pdt)_3]^0$,[57] $[W(pdt)_3]^0$,[58] and $[Re(pdt)_3]^0$,[59] which have all been shown to be trigonal prismatic by single crystal X-ray crystallography. This is of course not compelling. Quite to the contrary, we would like to argue that, in fact, $[Cr^{III}(tbbdt^{\bullet})_3]^0$ and $[Cr^{III}(pdt^{\bullet})_3]^0$ as was shown by broken symmetry BS(3,3) DFT calculations above, possess octahedral geometry ($\Theta_{calcd.} = 47.9°$ and 49.7°, respectively). According to these calculations the electronic structure is best described as containing a central Cr(III) d^3 ion and three antiferromagnetically coupled ligand π radical monoanions affording the observed $S = 0$ ground state. This holds for ligands of type A and B. Experimentally, this is corroborated by the electronic spectra of diamagnetic tris(*o*-semiquinonato)chromium (III)[60] and its analogous $[Cr^{III}(L'^{\bullet})_3]$ complex ($L'^{\bullet}$ = bis(2,6-diisopropylphenyl)glyoxal π-radical anion)[61] which have both been characterized by X-ray crystallography (octahedral CrO_6 polyhedra). The electronic spectra are quite similar; they display two very intense ($\varepsilon > 10^4$ M^{-1} cm^{-1}) transitions in the visible region at 450−500 and 470−530 nm. The same two transitions albeit at somewhat lower energies have been observed for $[Cr^{III}(tbbdt)_3]^0$ at 590 and 700 nm and for $[Cr(pdt)_3]^0$ at 581 and 686 nm.[2,4] Cr K-edge XAS for $[Cr^{III}(L_{SQ}^{\bullet})_3]$ has proven the presence of a central Cr(III) d^3 ion.[4] We conclude therefore that the same is probably true for the sulfur analogues.

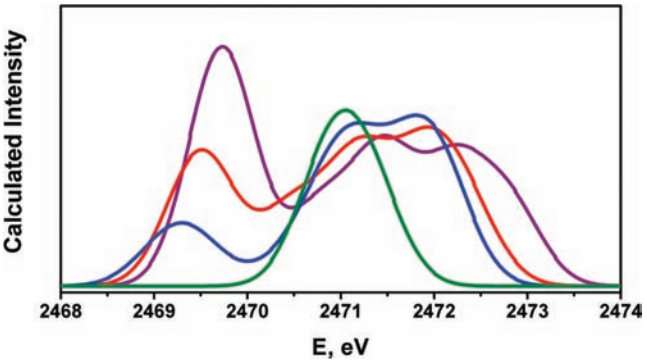

Figure 18. Calculated S K-edge XAS spectra for the four members of the electron transfer series $[Cr(tbbdt)_3]^z$ (z = 0 (purple), 1− (red), 2− (blue), 3− (green)) obtained from BP86 TD-DFT calculations. Calculated intensity in arbitrary units.

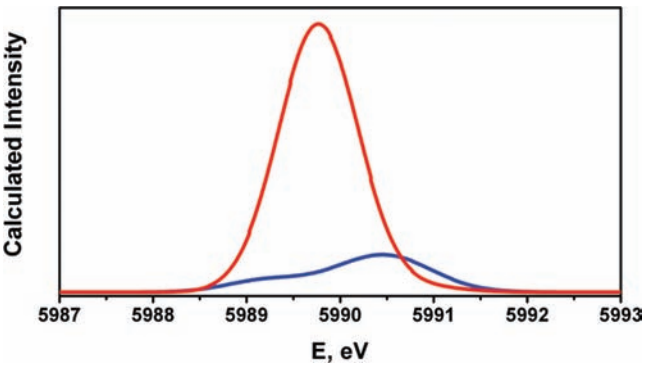

Figure 19. Calculated Cr K-pre-edge XAS spectra for the octahedral (blue) and trigonal prismatic (red) geometry optimized structures of $[Cr(pdt)_3]^0$. Calculated intensity in arbitrary units.

We have also calculated the S K-edge spectra of the series $[Cr(tbbdt)_3]^z$ (z = 0, 1−, 2−, 3−) as shown in Figure 18. The data for the monoanion $[Cr^{III}(tbbdt^{\bullet})_2(tbbdt)]^{1-}$ agree nicely with experiment.[4] It is gratifying that the calculated intensity of the low-energy transition is most intense for the neutral species, intermediate for the monoanion, and lowest for the dianion. This transition is absent in the spectrum of the trianion. Thus, the electronic structures of these members of the electron transfer series are best described as $[Cr^{III}(tbbdt)_3]^{3-}$, $[Cr^{III}(tbbdt^{\bullet})(tbbdt)_2]^{2-}$, $[Cr^{III}(tbbdt^{\bullet})_2(tbbdt)]^{1-}$, and $[Cr^{III}(tbbdt^{\bullet})_3]^0$. Furthermore, we have calculated the expected Cr K-pre-edge spectra for the octahedral and trigonal prismatic $[Cr(pdt)_3]^0$, and the plots overlaid in Figure 19 show a stark difference. The pre-edge intensity for the trigonal prismatic structure is ∼5 times more than the octahedral one. This arises from the significantly large Cr 4p character (4.2%) in the 5e′ MOs providing a dominating dipole contribution to this transition. Thus, the metal pre-edge is a useful spectroscopic marker for trigonal prismatic geometry as we will demonstrate in a forthcoming publication on tris(dithiolene) vanadium complexes.[56]

It is again very instructive to compare these results with the corresponding, neutral molybdenum derivatives with an $S = 0$ ground state. $[Mo(tbbdt)_3]^0$ and $[Mo(mdt)_3]^0$ have been

(56) Sproules, S.; Bill, E.; Weyhermüller, T.; DeBeer George, S.; Wieghardt, K., manuscript in preparation.
(57) Sproules, S.; Banerjee, P.; Bill, E.; Weyhermüller, T.; DeBeer George, S.; Wieghardt, K., manuscript in preparation.
(58) Goddard, C. A.; Holm, R. H. *Inorg. Chem.* **1999**, *38*, 5389.
(59) (a) Eisenberg, R.; Brennessel, W. W. *Acta Crystallogr.* **2006**, *C62*, m464. (b) Eisenberg, R.; Ibers, J. A. *J. Am. Chem. Soc.* **1965**, *87*, 3776. (c) Eisenberg, R.; Ibers, J. A. *Inorg. Chem.* **1966**, *5*, 411.
(60) Benelli, C.; Dei, A.; Gatteschi, D.; Güdel, H. U.; Pardi, L. *Inorg. Chem.* **1989**, *28*, 3089.
(61) Spikes, G. H.; Sproules, S.; Bill, E.; Weyhermüller, T.; Wieghardt, K. *Inorg. Chem.* **2008**, *48*, 10935.

structurally characterized;[42,54] they both possess a trigonal prismatic MoS_6 polyhedron. The S K-edge data of both species suggest the presence of π radical ligand(s) (one or two S valence holes, respectively).[42,43] Thus, for the benzene-1, 2-dithiolate derivative an electronic structure $[Mo^{V}(tbbdt^{\bullet})(tbbdt)_2]$ has been proposed given its very similar Mo L_2-edge spectrum to that of the monoanion. The Mo K-edge XAS data of both complexes are also virtually identical.[57] However, the S K-edge spectra of $[Mo(tbbdt)_3]^0$ and $[Mo(mdt)_3]^0$ are very similar, which led the authors in ref 43 to formulate the electronic structure as $[Mo^{IV}(tbbdt^{\bullet})_2(tbbdt)]^0$, the same as $[Mo^{IV}(mdt^{\bullet})_2(mdt)]^0$ with a type B ligand. It is clear that a $[Mo^{VI}(mdt)_3]^0$ or $[Mo^{VI}(tbbdt)_3]^0$ does not exist and that further experiments are necessary to unambiguously determine the electronic structure of neutral tris(dithiolene) molybdenum complexes.

Conclusion

We have synthesized and isolated three members of a previously unexplored electron transfer series, $[Cr(Cl_2\text{-}bdt)_3]^z$ (z = 1−, 2−, 3−) and shown through the combination of XAS and DFT calculations that each member contains an octahedral Cr(III) ion and are linked by successive one-electron ligand-centered redox processes. TD-DFT calculations have been successively employed to simulate the pre-edge regions of the Cr, Mn, and S K-edge spectra and facilitated a transition assignment. For the first time this has been extended to complexes with ground states derived from BS solutions such that we are confident in predicting the molecular and electronic structure for neutral tris(dithiolene) chromium as octahedral $[Cr^{III}(L^{\bullet})_3]$ complexes in line with dioxolene systems. With the electronic structure of this electron transfer series defined, we have begun to make meaningful comparisons to molybdenum analogues such that this series represents a benchmark for investigation into many tris(dithiolene) complexes of early transition metals.

Acknowledgment. We thank Dr. Eckhard Bill for simulating the EPR spectra. We are grateful for the financial support from the Fonds der Chemischen Industrie. P.B. and S.S. thank the Max-Planck-Society for postdoctoral stipends. SSRL operations are funded by the Department of Energy, Office of Basic Energy Sciences. The Structural Molecular Biology program is supported by the National Institutes of Health (Grant 5 P41 RR001209), National Center for Research Resources, Biomedical Technology Program and by the Department of Energy, Office of Biological and Environmental Research.

Supporting Information Available: Experimental details of the XAS measurements. X-ray crystallographic files in CIF format for **1**, **6**, and **7** and tables of geometric and electronic structure details (optimized coordinates, qualitative MO schemes, and Mulliken spin density plots) of BS DFT calculated structures for **1**−**9**, $[Cr(mnt)_3]^{1-}$, and $Cr(pdt)_3$. Magnetic susceptibility plots for **6**− **9**; electronic absorption spectra for **4**−**7**; cyclic voltammograms for **1**, **4**, **6**, and **7**; X-band EPR spectra and simulations for **2**, **3**, **6**, **9**, and $[Cr(mnt)_3]^{1-}$; pseudo-Voigt fits to the S K-edge spectra for **1**−**3**, **6**, and **7**, and fitting parameters for complexes 1−**9**. Figure S21 displays the calculated Cr K-pre-edge spectra for **4** and **5**. This material is available free of charge via the Internet at http://pubs.acs.org.